

**Inorganic
carbon dynamics
and CO₂ fluxes
in the Saguenay
Fjord (Québec,
Canada)**



McGill

LOUISE DELAIGUE
**DEPARTMENT OF EARTH AND PLANETARY
SCIENCES**

McGill University, Montreal - August 2018
*A thesis submitted to McGill University in partial
fulfillment of the requirements of the degree of
M.Sc.*

© Louise Delaigue (2018)

Table of Contents

Abstract	3
Résumé	4
List of Figures	5
List of Tables	7
Acknowledgments	8
Author Contribution	9
Chapter 1: Introduction	10
1. Fjords: background and environmental setting.....	10
1.1 Definition and distribution	10
1.2 Geomorphology, climate and important oceanographic characteristics	11
2. The Saguenay Fjord, Québec.....	14
2.1 Physical and geological characteristics.....	14
2.2 Hydrographic dynamics and circulation	19
2.3 Dominant sedimentation processes.....	24
3. Impetus for estuarine research.....	25
4. Thesis objectives.....	29
Connecting Text	30
Chapter 2: Spatial variations of the CO₂ fluxes in the Saguenay Fjord (Québec, Canada) and results of a water mixing model	31
Abstract	31
1. Introduction.....	32
2. Data and methods	33
2.1 Study site characteristics.....	33
2.2 Water-column sampling	36
2.3 Analytical procedures	37
2.4 Calculations	39
2.4.1 Water mass distribution analysis.....	39
2.4.2 Source-Water Type definitions	41

2.4.3 CO ₂ partial pressures	42
2.4.4 CO ₂ flux across the air-sea interface.....	43
2.4.5 Water mixing model	45
2.4.6 Salinity normalization of DIC in surface waters.....	46
2.4.7 Oxygen saturation and apparent oxygen utilization in the surface waters	47
3. Results and discussion.....	47
3.1 Water mass analysis	47
3.2 Aqueous pCO ₂ and CO ₂ flux.....	48
3.3 Water mixing model approach.....	53
4. Summary and conclusions.....	58
Acknowledgments.....	59
ANNEX: Additional information	60
Chapter 3: General summary and conclusions	61
References	64

Abstract

The Saguenay Fjord is a major tributary of the St Lawrence Estuary and is strongly stratified. A 6-8 m wedge of brackish water typically overlies up to 270 m of seawater. Despite all the research carried out to date, the mode, magnitude and frequency of water and carbon exchange between the estuary and the fjord remain unquantified. Relative to the St Lawrence River, the surface waters of the Saguenay Fjord are more acidic and host lower dissolved inorganic carbon (DIC) and higher dissolved organic carbon (DOC) concentrations. The surface waters of the fjord are projected to be a net source of CO₂ to the atmosphere. Nonetheless, the intrusion, at the surface, of brackish water from the upper estuary with the rising tide, as well as mixing of seawater, overflowing the sill from the lower estuary, below the pycnocline modulate the CO₂ dynamics in the Saguenay Fjord.

Using geochemical and isotopic tracers as well as an optimization multiparameter algorithm (OMP), we determined the relative contribution of known source-waters to the water column in the Saguenay Fjord, including deep waters that originate from the Lower St. Lawrence Estuary and replenish the fjord's deep basins. These results, when combined to a conservative (salinity, temperature, total alkalinity, dissolved inorganic carbon) mixing model and compared to field measurements, serve to identify the dominant factors, other than physical mixing, such as biological activity (photosynthesis, respiration) and gas exchange at the air-water interface, that impact the water properties (e.g., pH, pCO₂, nutrient concentration) of the fjord. Results indicate that the fjord's surface waters are a net source of CO₂ to the atmosphere during periods of high freshwater discharge (e.g., spring freshet) whereas the surface waters serve as a net sink of atmospheric CO₂ when their salinity exceeds ~ 5-10.

Résumé

Le fjord du Saguenay est un tributaire majeur de l'estuaire du Saint-Laurent et est fortement stratifié. Une couche d'eau saumâtre de 6-8 m recouvre généralement jusqu'à 270 m d'eau de mer. Malgré toutes les recherches effectuées à ce jour, le mode, l'ampleur et la fréquence des échanges d'eau et de carbone entre l'estuaire et le fjord ne sont pas quantifiés. Comparativement au fleuve Saint-Laurent, les eaux de surface du fjord du Saguenay sont plus acides et contiennent moins de carbone inorganique dissous (CID) et plus de carbone organique dissous (COD). Les eaux de surface du fjord devraient constituer une source nette de CO₂ vers l'atmosphère. Néanmoins, l'intrusion, en surface, d'eaux saumâtres de l'estuaire fluvial avec la marée montante, ainsi que le mélange d'eau de mer, débordant du seuil de l'estuaire maritime sous la pycnocline, modulent la dynamique du CO₂ dans le fjord du Saguenay.

A l'aide de traceurs géochimiques et isotopiques ainsi que d'un algorithme d'optimisation multiparamétrique (OMP), nous avons déterminé la contribution relative des sources connues à la colonne d'eau du fjord du Saguenay, y compris les eaux profondes provenant de l'estuaire maritime du Saint-Laurent et qui renouvellent les eaux des bassins profonds du fjord. Ces résultats, combinés à un modèle de mélange conservateur (salinité, température, alcalinité totale, carbone inorganique dissous) et comparés aux mesures sur le terrain, permettent d'identifier les facteurs dominants, autres que le mélange physique, tels que l'activité biologique (photosynthèse, respiration) et les échanges gazeux, qui influencent les propriétés des eaux (par exemple, pH, pCO₂, concentration en nutriments) du fjord. Les résultats de cette étude indiquent que les eaux de surface du fjord sont une source nette de CO₂ pour l'atmosphère pendant les périodes de fort apport en eau douce (par exemple, crues printanières) alors que les eaux de surface servent de puits net de CO₂ atmosphérique lorsque la salinité excède ~ 5-10.

List of figures

▪ Chapter 1: Introduction

Fig. 1 a) Bathymetry and geographic location of the Saguenay Fjord. **b)** Longitudinal section of the Saguenay Fjord, showing the strong halocline. The approximate locations of the following are shown: Tadoussac (TA), L'Anse de Roche (ASDR), Baie Sainte-Marguerite (BA), Anse-Saint-Jean (ASJ), Baie-Eternité (BE), St. Fulgence (SF), Baie des Ha! Ha! (BHA). 15

Fig. 2 a) Overview of the Saguenay Fjord. Point A to point B: Lower Saguenay. Point B to point C: Middle Saguenay. Point C to point D: Upper Saguenay, including the Baie des Ha! Ha! **b)** Lower Saguenay, from point A to point B. APS: Anse Petit Saguenay; BSM: Ste. Marguerite Bay; BSE: St. Étienne Bay; PI: Des Petites Iles Point. **c)** Upstream part of the North Arm (Bras-Nord) showing mass movement signatures and ripples, and upper ridges of the Baie des Ha! Ha! **d)** Lower Saguenay, from point A to point B. APS: Anse Petit Saguenay; BSM: Ste. Marguerite Bay; BSE: St. Étienne Bay; PI: Des Petites Iles Point (modified from Locat *et al.*, 2008)..... 19

Fig. 3. Schematic representation of the Saguenay Fjord general water circulation. White arrows illustrate the estuarine circulation, with surface current going in downstream direction. Black arrows illustrate the dense coastal inflow circulation, with deep currents going in the upstream direction. The approximate location of the following are shown: Tadoussac (TA), L'Anse de Roche (ASDR), Baie Sainte-Marguerite (BA), Anse-Saint-Jean (ASJ), Baie-Eternité (BE), St. Fulgence (SF), Baie des Ha! Ha! (BHA) 21

Fig. 4. Three proposed water-mass renewal regimes in the Saguenay Fjord. Top: deep winter renewal; middle: winter subsurface renewal; bottom: intermediate summer renewal (Belzile, Galbraith, and Bourgault, 2016) 23

Fig. 5. a) Surface areas of estuaries, continental shelves and open oceans and **b)** their estimated air-water CO₂ fluxes. From Cai (2011) 26

▪ Chapter 2: Spatial variations of the CO₂ fluxes in the Saguenay Fjord (Québec, Canada) and results of a water mixing model

Fig. 1 a) Bathymetry and geographic location of the Saguenay Fjord. Red dots represent the hydrographic stations sampled in the Saguenay Fjord during R/V Coriolis II cruises. **b)** Longitudinal section of the Saguenay Fjord, showing the strong halocline. The approximate location of the following are shown: Tadoussac (TA), L'Anse de Roche (ASDR), Baie Sainte-Marguerite (BA), Anse-Saint-Jean (ASJ), Baie-Eternité (BE), St. Fulgence (SF), Baie des Ha! Ha! (BHA) 35

Fig. 2 a) Practical salinity (S_p) versus measured alkalinity ($TA_{(meas)}$) for SRW and CIL data points, for all sampling months ($R^2 = 0.99$). The yellow triangle defines the properties of the SRW, and the dark blue square comprises the properties of the CIL. **b)** $TA_{(meas)}$, $TA_{(calc)}$ and Org Alk definitions for the Saguenay River (SRW), using surface data from all sampling months, with standard error 45

Fig. 3. Vertical sections showing the relative contributions of the Saguenay River (SRW), the St. Lawrence Estuary cold intermediate waters (CIL) and Lower St. Lawrence Estuary bottom waters (LSLE) to the water column structure of the Saguenay Fjord (June 2017). Fractions were estimated using an Optimum Multi-Parameter (OMP) algorithm, (Tomczak and Large 1989; Tomczak 1981; Mackas and Harrison 1997)). A Variational Analysis (DIVA) interpolation was applied between field data points in Ocean Data View **48**

Fig. 4. Spatial distribution of surface-water $p\text{CO}_{2\text{sw}}$ in June 2017, November 2017, May 2016 and September 2014. The red line represents the $p\text{CO}_{2(\text{air})}$ for each year. Data points above the red line indicate that waters are sources of CO_2 to the atmosphere, whereas those below the red line identify waters that are sinks of atmospheric CO_2 **50**

Fig. 5 a) Spatial distribution of air-sea CO_2 flux ($\text{mmol}\cdot\text{m}^{-2}\cdot\text{d}^{-1}$) in the Saguenay Fjord surface waters for all cruises. Data points above the red line indicate sources of CO_2 to the atmosphere, whereas those below the red line are sinks of atmospheric CO_2 . **b)** Spatial interpolation of air-sea CO_2 fluxes ($\text{mmol}\cdot\text{m}^{-2}\cdot\text{d}^{-1}$) in the Saguenay Fjord surface waters for all cruises. Red triangles indicate sampling locations **52**

Fig. 6 Box-plot for the air-sea CO_2 fluxes from all data in the two subdivisions of the study area (Inner basin and Outer basins). The red line is the median, the box spans the interquartile range (25-75 percentiles) and the whiskers show the extreme data points not considered outliers. One outlier is identified by the + symbol **53**

Fig. 7 Results of the conservative, two end-member mixing model for $p\text{CO}_{2(\text{SST})}$ in the Saguenay Fjord surface waters. Dashed lines represent the $p\text{CO}_{2(\text{air})}$ on the sampling months (respectively 396 ppm in September 2014, 407ppm in May 2016, 408 ppm in June and November 2017) **54**

Fig. 8 Spatial distribution of surface-water dissolved O_2 saturation in June 2017, November 2017, May 2016 and September 2014. The red line represents equilibrium. Data points above the red line indicate that waters are supersaturated in O_2 , whereas those below the red line identify O_2 -undersaturated waters with respect to the atmosphere **55**

Fig. 9 a) ΔNDIC distribution in the Saguenay Fjord surface waters. Data were normalized to a common salinity (average for each sampling period) according to Friis *et al.* (2003); **b)** Comparison of the apparent oxygen utilization (AOU) and ΔNDIC **57**

ANNEX: Fig. A Salinity versus a) Temperature, b) Total Alkalinity (TA), c) Dissolved Inorganic Carbon (DIC), d) $\delta^{18}\text{O}_{\text{water}}$, e) Dissolved Oxygen (DO), and f) DSi for data from September 2014, May 2016, June 2017 and November 2017 from R/V Coriolis II cruises. Each large symbol (square, circle, triangle and star) represents distinct source-water masses..... **60**

List of tables

- **Chapter 2: Spatial variations of the CO₂ fluxes in the Saguenay Fjord (Québec, Canada) and results of a water mixing model**

Table 1. Source-Water Type (SWT) definitions for the Saguenay River (SWR), the St. Lawrence Estuary summertime Cold Intermediate Layer (CIL), the Lower St. Lawrence Estuary bottom water (LSLE) and the St. Lawrence River (SLRW). Definitions were derived from data taken in September 2014, May 2016, June 2017 and November 2017. Data for SRW and SLRW were extrapolated to $S_p = 0$. The weights used in the OMP analysis are also shown **41**

Table 2. Mean, standard error and range of pCO₂, K, u and F in the Saguenay Fjord surface waters. Numbers in parentheses indicate the ranges observed or estimated **51**

Table 3. Area-averaged, air-sea CO₂ flux (mmol·m⁻²·d⁻¹) estimates for each subsection of the Saguenay Fjord, for N data points, per sampling month. The fjord was divided into two subsections. The 'Inner basin' segment encompasses the 30-100 km section from the mouth of the fjord (Fig. 1b), whereas the 'Outer basins' segment includes the 0-30 km section. The whole fjord CO₂ flux was computed by combining all available flux data over the four sampling months **51**

Acknowledgments

First and foremost, I would like to thank my supervisor, Dr. Alfonso Mucci, and the Department of Earth and Planetary Sciences at McGill University for research and financial support.

I had the privilege and pleasure to be supervised by Al Mucci. I wish to thank him for his patience and precious time. Working with Al gave me the opportunity to work on several different projects and participate in numerous oceanographic research expeditions in the Estuary and Gulf of St. Lawrence as well as the Canadian Arctic. I was also lucky to present my work at the Ocean Science Meeting (OSM) in Portland (Oregon), as well as the Canadian Meteorological and Oceanographic Society (CMOS) congress in Halifax (Nova Scotia). I am grateful for access to the diverse datasets used in this thesis, and the more than helpful and fruitful scientific discussions with Al throughout these two years.

I am also indefinitely thankful to Constance Guignard for her never-ending patience and expertise on lab analysis; to the SECO.Net team for their precious mentoring and infallible good mood; and to Gilles Desmeules, the captains and crew of the R/V Coriolis II, without whom sampling would have been impossible.

I would also like to thank everyone in our research group, past and present – Olivier Sulpis, Will Nesbitt, Mathilde Jutras, Alexis Beaupré-Laperrière, Pascale Daoust and Ashley Dinauer – for their never-ending support and encouragement. They were all present in times of fun, excitement and discovery as much as doubt, seasickness and exhaustion. I must also express my gratitude to my mom and sisters, my dad, family, J.B., Mr. K. and the Valenta family, Quenten, along with friends – Becky, Cat, Eva and Hannelore – who experienced the ups and downs of my graduate research and who faithfully and loyally supported me throughout my personal and academic life. I dedicate this thesis to them.

Author contribution

The results of this thesis are presented in the form of one co-authored paper. The authors of the paper are in the following order: Louise Delaigue, Helmuth Thomas and Alfonso Mucci. The data analysis, model development, the interpretation and synthesis of the results, the production of the figures, and the writing were done by the author of the thesis. Dr. Thomas contributed to the research by providing results of alkalinity and dissolved inorganic carbon analyses carried out at Dalhousie University (Nova Scotia). Dr. Mucci contributed by collecting the oceanographic data as well as supervising and reviewing the work.

Chapter 1: Introduction

1. Fjords: background and environmental setting

1.1. Definition and distribution

A fjord is most often defined as a narrow arm of sea, with steep sides and high bathymetry, eroded from a melting glacier. Fjords typically have a free connection to the open sea and within which seawater is measurably diluted with freshwater derived from land drainage, therefore forming a semi-enclosed coastal body of water (Pritchard, 1967). In other words, fjords can be seen as a type of estuary, characterized by an estuarine circulation pattern involving a degree of haline stratification of the water column. Fjords are the youngest, deepest type of estuaries, and generally stem from the retreat of ice and sea level fluctuations that have ensued since the last glacial maximum (17,000 years BP). These transient systems evolve over short time scales (centuries to millennia) and are typically sites of net sediment accumulation in mountainous regions.

Canada hosts a large number of fjords as it displays one of the largest coastlines in the world. Canadian fjords are exceptionally diversified, and their characteristics range from low to high sediment rate, tide- or wave-dominated to river-dominated, continually oxygenated to permanently anoxic, and from temperate drainage basins, free of snow and ice, to frigid, permanently ice-covered inlets (Syvitski et al., 1987). The East Coast of Canada includes about 200 fjords, with 100 located in Newfoundland, 60 in Labrador, 35 in Nova Scotia, and 5 in Québec. Interestingly, the Northern Gulf of the St. Lawrence is considered the longest infilled paleofjord coast, as it combines a large drainage basin (10^4 to 10^5 km²) with traces of rapid infill, and has undergone little change since the last deglaciation (Syvitski et al., 1987). Québec encompasses fewer fjords than other coastal provinces in Canada due to the high isostatic rebound (120-200 m) and rapid fjord infill that occurred at the end of the last deglaciation (Syvitski et al., 1987). Québec inlets include the Saguenay Fjord, the Baie de Gaspé, Grand-Lac-Salé, the Gros Mecatina River, and Baie de Jacques-Cartier. The Saguenay Fjord is an example of a classical fjord. It includes a deep basin (275 m), a shallow sill (20 m), a major fjord-head fluvial input (the Saguenay River), and displays a 2-layer estuarine circulation (Fig. 3; Côté and Lacroix, 1978; Sundby and Loring, 1978). Sedimentation rates decrease exponentially seaward, from 10 cm yr⁻¹ at the

Saguenay River discharge near St. Fulgence to 0.1 cm yr^{-1} near its mouth (Smith and Schafer, 1985). The Saguenay Fjord is the focus of the study presented in the manuscript accompanying this thesis.

1.2. Geomorphology, climate and important oceanographic characteristics

The formation of fjords is closely related to the local glacial and paraglacial history. Accordingly, most of the sediment accumulation from glacial erosion and deposition within fjord inlets are due to proglacial infilling during and after the last major ice advance (Aarseth et al., 1975; Gilbert, 1985). Generally, fjords enclose submarine sills that delineate the inlet's internal basins and modulate the distinctive physical and biogeochemical processes that occur within it. Those inlets are only found within coastal terrains that were once dominated by Quaternary ice sheets (Holtedahl, 1967). Their origin therefore depends on fluvial action along fault lines, coupled with subsequent excavation by glaciers as melt waters follow the path of least resistance (Syvitski et al., 1987). As a result, a major freshwater inflow is commonly found at the head of the fjord, along with a brackish surface plume flowing seaward. Fjords are transition regions between land and open oceans, where strong physical and chemical gradients are observed. These gradients are also seen in the sediments, as coarser, fluvially transported sediment is typically found in the upper parts of fjords while finer material is observed closer to the mouth (Gade and Edwards, 1980).

The geomorphology of fjords is closely related to the local geological, climatological, and glacial/post-glacial conditions. Typically, a fjord is described as a U-shape valley, located in a glaciated, mountainous terrain (Gilbert, 1985). The subaerial profile of a fjord will be contingent on the degree of regional erosion. The latter will depend on the thickness of the ice sheet, slope, plasticity of the ice, basal thermal regime of the glacier, bedrock friction and friability (Boulton, 1982). The dominant sedimentary process will define the submarine cross-section profile of the fjord. For instance, a high sedimentary rate coupled with weak bottom currents will lead to the accumulation of a conformable layer of sediment infill deposited as bottom bathymetry (Syvitski et al., 1987). Morainal and glaciomarine deposits form sills, separating fjords into several basins (Brodie, 1964).

The presence of a shallow sill and strong stratification can restrict water exchange with the open ocean and lead to the development of deep-water stagnation as well as dissolved oxygen depletion (Richards, 1965). According to Molvær (1980), the water exchanged during renewal events does not generally replace the entire volume of the fjord's bottom water, but rather anywhere from 20% to 80% of the total volume of water. Therefore, the presence of sills often leads to periods of water-mass stagnation – including surface waters - within the fjord, but the energy provided by tides generates turbulence for vertical mixing that can counterbalance stagnation (Gade, 1968). The amount of turbulence generated by tides, however, differs among fjords over the world. For example, vertical diffusivities in the deep waters in fjords of British Columbia range from 10^{-5} to $3 \times 10^{-3} \text{ m}^2 \text{ s}^{-1}$ (Smethier, 1981), whereas lower vertical diffusivities, on the order of $10^{-6} \text{ m}^2 \text{ s}^{-1}$, are observed in Norwegian fjords (e.g., Framvaren Fjord) (Gade and Edwards, 1980). The tidal amplitude has a noticeable impact on sediment transport and deposition in fjords, resuspending sediments along the shores to deposit them in lower energy, often deeper, areas. Tidal amplitudes vary greatly, from practically 0 meters in southern Norway to 10 meters in Cook Inlet (Alaska).

Climatic variations control glaciation and deglaciation cycles, and hence changes in sea level: climate is therefore responsible for the origin and distribution of all types of estuaries (Schubel and Hirschberg, 1978). Climate variability heavily influences morphology and sediment input, by controlling the rates of weathering of rocks, sediment yields, and vegetation development in a given catchment area. Water temperature as well as the amount and type of precipitation are also governed by climate, and further determine the style of estuarine circulation in the fjord. The climate of fjords varies from Arctic desert to temperate maritime. Areas where precipitation falls as snow yield a heavy spring freshet, heavily impacting a fjord's general circulation (e.g., Saguenay Fjord, Québec). In climates allowing for the formation of glaciers, glacier melt favors the transport of a high suspended-sediment load. In flood periods, sediment pulses are often observed, leading to a discrete layer of sediment on the seafloor (Glasby, 1978). A layer of ice may develop during the winter months, leading to a decrease in sediment flux by 90% to 95%, as well as an interruption of shallow-water sediment resuspension and supply of sediment to the deeper basins due to wind inhibition (Skei, 1983). The influence of

wind is also notable, as it is the primary actor in the resuspension of shallow deposits and breakdown of the water column stratification in upper waters because of waves and turbulence. Strong winds blowing landward will also impact the brackish surface layer by slowing down its flow, further diminishing the dispersal of sediment and increasing the residence time of the surface waters within the fjord (Syvitski et al., 1987). Climate is therefore a ruling factor in fjord systems, specifically with respect to topography, water column stratification and vegetation/soil cover.

One of the key oceanographic characteristics of a fjord is the ability of seawater to be measurably diluted with freshwater derived from land drainage (Pritchard, 1967). The estuarine circulation is classified according to the degree of haline stratification of the water column. The level of stratification depends on the balance between the amount of denser and saltier waters delivered by processes such as tidal movement, and the discharged freshwater (Syvitski et al., 1987). The typical circulation of a fjord consists of a two-layer flow with an outward-flowing brackish surface layer overlying a dense, salty inward-moving compensating current (d'Anglejan and Smith, 1973). This type of flow maximizes sedimentological and biogeochemical gradients (Syvitski and Murray, 1981).

Strong physical-chemical gradients develop in some fjords, i.e. will be fully oxygenated in the surface waters and close to anoxic in the deepest part of the basins. The oxygen regime depends on the frequency and magnitude of water exchange, the oxygen demand (respiration rate), and the supply of organic matter. For a fjord with deep sills and frequent water exchange, the oxygen saturation depth will lie above the pycnocline, with a slight undersaturation at depth caused by organic matter breakdown and poor water movement (Syvitski et al., 1987). Mixing between freshwater and marine water is also accountable for the oxygen content in the surface waters. An oxygen minimum is often observed at mid-depths in the water column, most often caused by the presence of a water mass within which mineralization processes are active, or due to the vertical displacement of low-oxygen waters following deep-water renewals (Syvitski et al., 1987). The residence time of the bottom waters is critical with respect to their oxygen content. The frequency of oxygen replenishment varies (diurnally, seasonally, episodically) depending on fjords, and bottom-water renewals usually occur when the density of waters at the sill depth is

greater than the density of water inside the basin, making the sill depth and density of waters outside the fjord critical factors. A fjord inlet combining a shallow sill and a long bottom-water residence time will tend to be anoxic, leading to the reduction of nitrate, sulfate and the accumulation of hydrogen sulfide in the water column (Richards, 1965). A maximum of 8 mmol H₂S was recorded in the Framvaren fjord, Norway (Richards, 1965; Skei, 1983; Strøm, 1936).

These miniature oceans provide unique opportunities to study terrestrial input into a quasi-closed marine system, as the inputs and outputs are easily measured. They serve as natural laboratories to study the migration of the redox gradients, the solubilization and precipitation of major and minor seawater constituents, as well as the cycling of carbon, nitrogen and trace metals. Fjords are therefore unique oceanographic environments and valuable assets for estuarine research.

2. The Saguenay Fjord, Québec

2.1 Physical and geological characteristics

Located in the subarctic region of Québec, eastern Canada, the Saguenay Fjord is up to 275 m deep, 110 km long and has an average width of 2 km, with a 1.1 km wide mouth where it connects to the head of Lower St. Lawrence Estuary (Fig. 1a). It is hypothesized that the geological origin of this unique valley is associated with the Grenville orogeny, a collision associated with the assembly of the supercontinent Rodinia and the buildup of the Laurentian hills in the mid to late Mesoproterozoic age (1250-980 Ma) during the Precambrian era (Tollo et al., 2004).

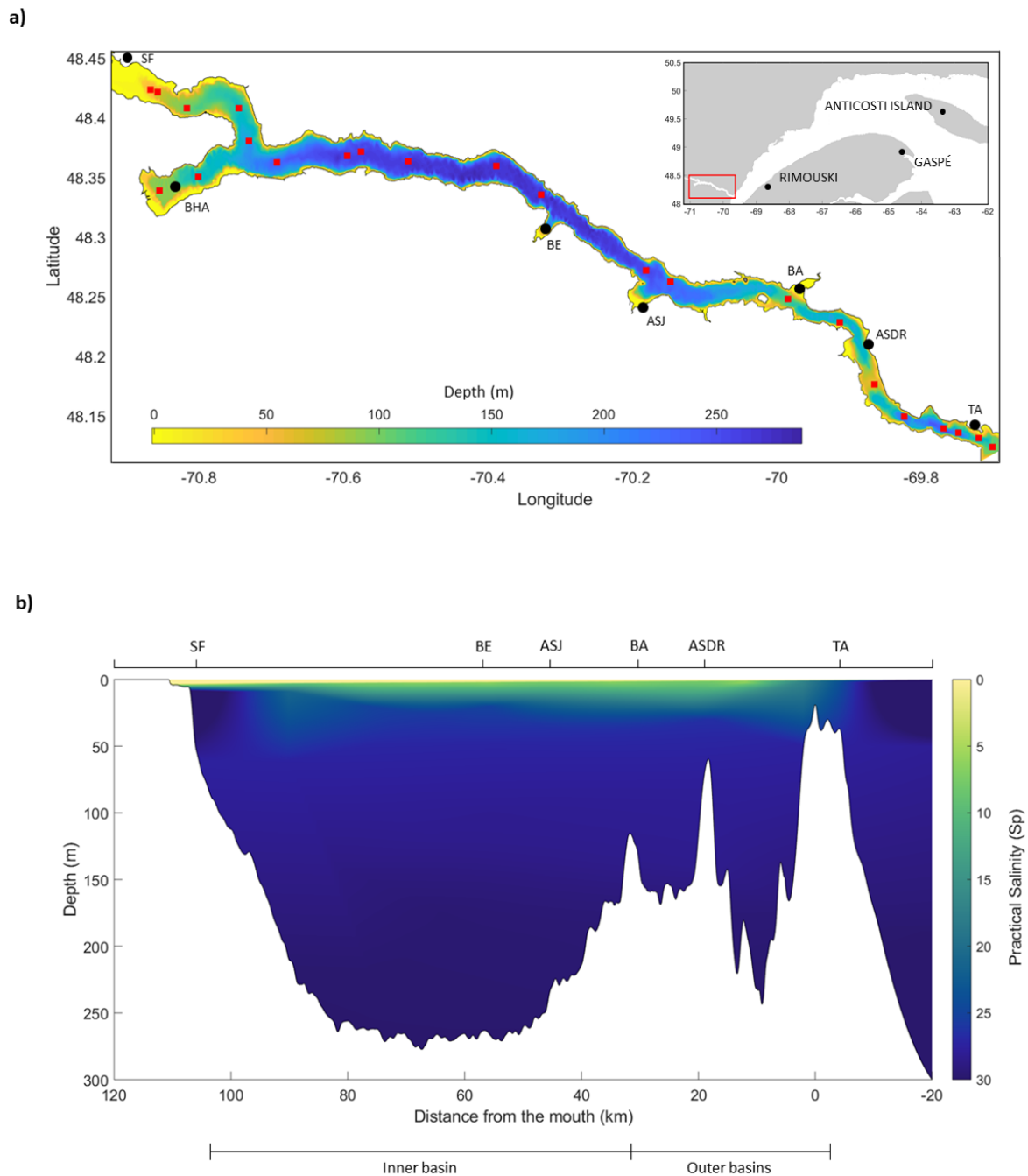


Fig. 1 a) Bathymetry and geographic location of the Saguenay Fjord. **b)** Longitudinal section of the Saguenay Fjord, showing the strong halocline. The approximate locations of the following are shown: Tadoussac (TA), L'Anse de Roche (ASDR), Baie Sainte-Marguerite (BA), Anse-Saint-Jean (ASJ), Baie-Eternité (BE), St. Fulgence (SF), Baie des Ha! Ha! (BHA).

The fjord's bathymetry includes three basins bound by three sills (Fig. 1b). The first one, at a depth of ~20 m, is located at its mouth near Tadoussac. It controls the overall dynamics of the fjord. The second is located 18 km further upstream and sits at a depth of 60 m, while the third is found another 32 km upstream and rises to a depth of 115m. The fjord's drainage basin is 78,000 km² (Smith and Walton, 1980) and is part of the larger St. Lawrence drainage basin, a hydrographic system that includes the Great Lakes and covers 1.36 million km².

The hydrography of the St. Lawrence system is mostly dominated by the Great Lakes (245,000 km²) and drains more than 25% of the Earth's freshwater reserves. It includes Lakes Michigan, Superior, Huron, Erie, Ontario and St. Clair. Most of the drainage occurs on the Canadian side of the border, in the Canadian Shield, and on a smaller scale, the St. Lawrence Lowlands (i.e. peninsular Ontario, St. Lawrence River). Rivers located in the lowlands are most often less than 300 km long but contribute greatly to the socio-economic development of the urban population along their shores (i.e. important for industry, agriculture and water supply). The average flow along the drainage basin varies from 5,760 m³ s⁻¹ (Niagara River, Queenston) to 9,800 km³ s⁻¹ (Ottawa River confluence, near Montreal). The Appalachian Mountains exhibit a smooth topography on the south shore of the St Lawrence River, while the Grenvillian metamorphic rocks, part of the Canadian Shield, rise steeply on the north shore, and reach an altitude over 1000 m south of the Saguenay Fjord – explaining most of the drainage pattern on the Canadian side (Pinet et al., 2011).

Because of the contrasting bathymetry and its impact on hydrodynamic conditions, sedimentary conditions vary sharply between the Lower (from Tadoussac to Pointe-des-Monts) and Upper Estuary (from Tadoussac to Québec City, including saltwater intrusions south-west of the Saguenay Fjord). The Upper Estuary (of interest, as closest to the Saguenay Fjord) is shallow and greatly affected by bedload reworking currents, preventing deposition of Holocene fine-grained sediments (Pinet et al., 2011). The landscape is also dominated by the Canadian Shield, with igneous and metamorphic rocks (granite, gneiss, pegmatite), as well as meta-sediments (schists, mica schists, gneisses), occupying about 80% of the area (Dionne and Occhietti, 1996). The Precambrian floor covers the Saguenay Fjord, as well as the north shore of the St Lawrence Estuary on either side of Tadoussac, as well as Baie Sainte-Catherine.

The St. Lawrence Estuary hosts Quaternary sediments with thicknesses ranging from less than 30 m to more than 400 m (Pinet et al., 2011). Sediments of the Saguenay Fjord also record a history of Quaternary sedimentary processes, indubitably linked to the St. Lawrence's. The mouth of the fjord is characterized by an original morpho-sedimentary raised delta (120-125 m wide) near Tadoussac, as well as a thick fluvio-marine valleyfill near Rivière-du-Moulin (Dionne and Occhietti, 1996). Complex terraces have also been documented near Pointe-aux-Vaches (60 m high) and Pointe-aux-Alouettes, as well as wide silty-clayey rhythmite terraces near Pointe Hubert and Pointe-aux-Bouleaux (Dionne and Occhietti, 1996). This area was most likely ice free during the Wisconsin interstadial, as 35,000 ka old shell fragments were found in the area of Pointe-aux-Alouettes. A period of sand and gravel deposition as well as marginal ice shelf deposition likely followed (Dionne and Occhietti, 1996). Around 10.4 ka, the Goldthwait Sea submerged the ice-free depressions of the Shield, making the Laurentide Ice Sheet retreat and thin on the highlands, and leaving an ice cover in the fjord that further eroded the valley, which isostatically recovered by 8 ka (Dionne and Occhietti, 1996). The Saguenay Fjord now shows steep and rocky banks that reach between 150 and 300 m in height above sea-level, much like many Norwegian fjords, with an uneven bottom including umbilics and thresholds of thick deposits (Drainville, 1968; Schafer et al., 1983).

As described by Locat et al. (2009), the Saguenay Fjord can be divided into three physiographic units: Lower, Middle, and Upper Saguenay (Fig. 2b). These units facilitate the interpretation of spatial data in their individual context. The Lower Saguenay Fjord extends from Tadoussac to the western part of Saint-Louis Island (Fig. 2a). This portion of the Saguenay Fjord is characterized by strong longitudinal, subparallel moraine deposits originating from glacial retreat, about 11,000 years BP. Outwash deposits are also present in the lee of Saint-Louis Island, which could have been an anchor point for the retreating glacier during the fjord's deglaciation 11,000 years ago (Locat and Levesque, 2009). There are also many minor but notable sills, some of which were previously mentioned, whose depths vary down to 240 m (Fig. 2b). The literature suggests a long period of glacial stagnation, as the moraine deposits are ~90 m thick, whereas the northern part of the lower portion (i.e., Sacré-Coeur region) appears to host a significant amount of marine sediments (Locat and Levesque, 2009; Syvitski and Praeg, 1989).

The boundary between the Lower Saguenay and Upper Saguenay is associated with a sharp bathymetric gradient, interpreted as evidence for the presence of ice during the last glaciation that prevented marine sediments from accumulating in the middle portion of the fjord (Fig 2b; Locat and Levesque, 2009). This interpretation is further supported by the absence of fine sediments in the deepest part of the lower fjord (i.e. near the mouth), and the irregular morphology of the Lower Saguenay.

According to the designated physiographic framework, the Middle Saguenay is the longest portion of the fjord. It runs from the eastern limit of the Lower Saguenay to the confluence of the North Arm (Bras-Nord) and the Baie des Ha! Ha! (Fig. 2a). Just like the boundary between the Lower and Middle Saguenay, the eastern limit of the Middle Saguenay is associated with an underwater cliff (Locat and Levesque, 2009). This portion of the fjord is also characterized by scars and remnants of landslides that were potentially triggered by an earthquake in 1663, which caused the collapse of the basin (Locat and Levesque, 2009; Syvitski and Schafer, 1996). These submarine landslides scar the edges of the Middle and Upper Saguenay, except between Anse-Saint-Jean and Saint-Basile-de-Tableau (Fig. 2d). Finally, the Upper Saguenay portion of the fjord that includes the North Arm (Bras-Nord) as well as the Baie des Ha! Ha! is considered a sediment trap. Important subaquatic ripples can be observed starting at the western end of the Upper Saguenay and into the Bras-Nord (Fig. 2c). The latter is characterized by a discontinuous channel and steep walls marked by numerous scars of submarine landslides (Locat and Levesque, 2009). The Baie des Ha! Ha! was also affected by the magnitude 8 earthquake of 1663, as it shows a mega-ripple due to the accumulation of sediment from the event (Fig. 2c; Locat and Levesque, 2009). In fact, a meter-thick rapidly deposited layer matching the record of the 1663 earthquake was identified: sediment cores recovered in this region reveal the presence of an unbioturbated, homogeneous light gray layer, and an increase in inorganic carbon content (CaCO_3) (St-Onge and Hillaire-Marcel, 2001; St-Onge et al., 2004; Syvitski and Schafer, 1996). Additionally, sediment texture and colour appear similar to other cores recovered in that area (St-Onge and Hillaire-Marcel, 2001; St-Onge et al., 2004; Syvitski and Schafer, 1996).

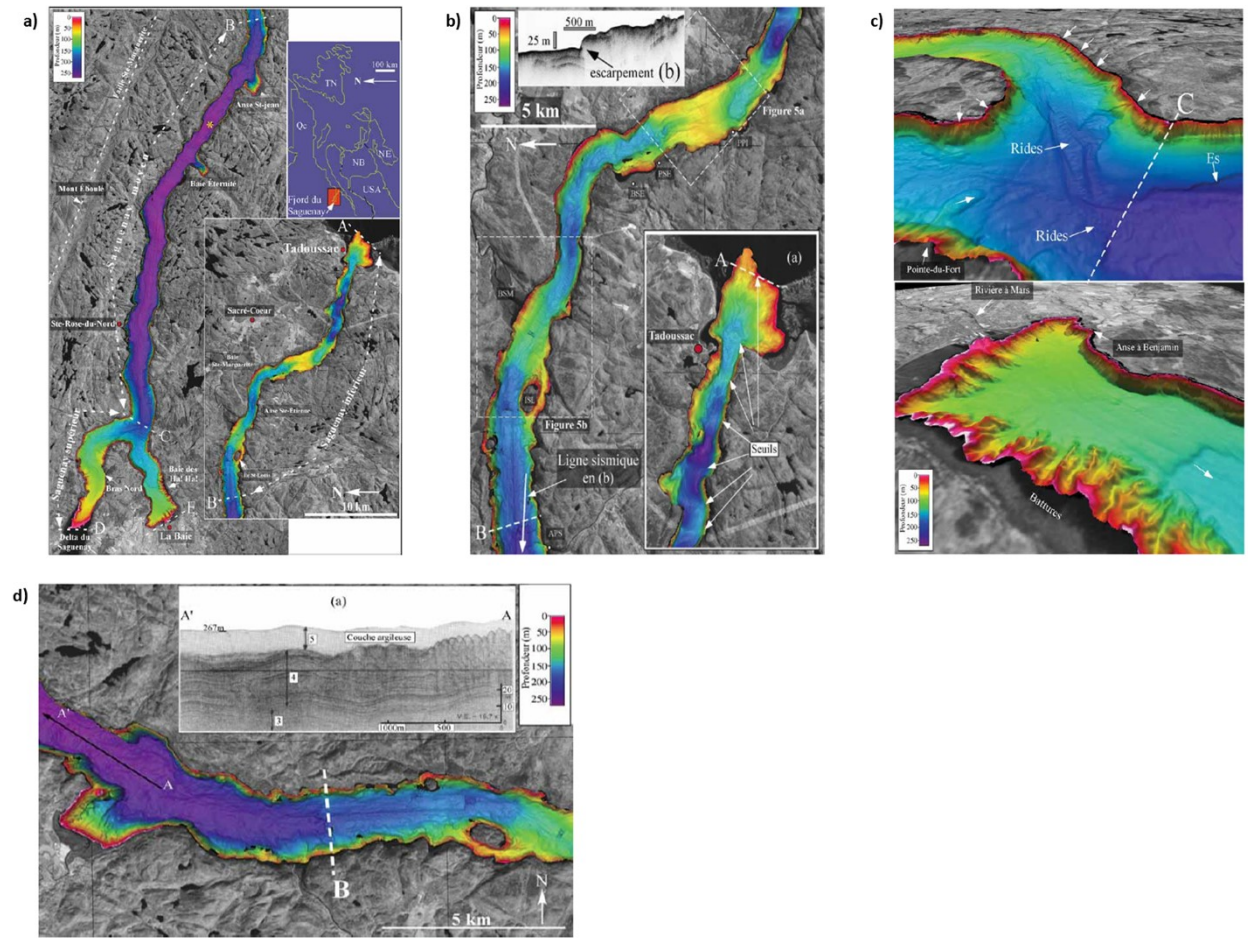


Fig. 2 a) Overview of the Saguenay Fjord. Point A to point B: Lower Saguenay. Point B to point C: Middle Saguenay. Point C to point D: Upper Saguenay, including the Baie des Ha! Ha! **b)** Lower Saguenay, from point A to point B. APS: Anse Petit Saguenay; BSM: Ste. Marguerite Bay; BSE: St. Étienne Bay; PI: Des Petites Iles Point. **c)** Upstream part of the North Arm (Bras-Nord) showing mass movement signatures and ripples, and upper ridges of the Baie des Ha! Ha! **d)** Lower Saguenay, from point A to point B. APS: Anse Petit Saguenay; BSM: Ste. Marguerite Bay; BSE: St. Étienne Bay; PI: Des Petites Iles Point (from Locat et al., 2009).

2.2 Hydrographic dynamics and circulation

Tributaries to the Saguenay Fjord include the Saguenay, Éternité and Sainte-Marguerite Rivers (Fig. 1b). The Saguenay River is the main outlet from the Saint-Jean Lake, and discharges into the North Arm of the fjord near St. Fulgence (Fig. 1b). Two other local, minor tributaries, the Rivière-à-Mars (95 km long, mean discharge $\sim 8 \text{ m}^3 \text{ s}^{-1}$) and the Rivière Ha! Ha! (35 km long, mean

discharge $\sim 15 \text{ m}^3 \text{ s}^{-1}$) discharge into the Baie des Ha! Ha!, a distinct feature of the Saguenay Fjord. Finally, the fjord receives denser marine waters from the St. Lawrence Estuary, filling the three basins, as these episodically overflow the entrance sill (Bélanger, 2003; Belzile et al., 2016; Stacey and Gratton, 2001; Therriault and Lacroix, 1975).

The Saguenay River is the most influential tributary to the fjord, with a mean fresh water discharge of $\sim 1200 \text{ m}^3 \text{ s}^{-1}$ (Bélanger, 2003). The overflow and the intrusion of marine waters from the St. Lawrence Estuary generate a sharp halocline, leading to a simplified description of the water stratification in the fjord (Fig 1.b): a thin brackish surface layer (5-10 m, $S_p \sim 10$; where S_p stands for practical salinity) overlying a denser layer ($S_p \sim 30$) of marine waters (Belzile et al., 2016). The tidally-modulated intrusion of marine waters from the St. Lawrence Estuary into the Saguenay Fjord, as well as the outflow of the fjord into the estuary, have a major influence on the water column stratification and circulation in the Saguenay Fjord and at its mouth. In other words, the properties of the uppermost 100 m of the water column in the adjacent estuary are critical in determining the water stratification in the Saguenay Fjord, since salinity and temperature control the density of waters that spill over the sill and fill the fjord's deep basins (Belzile et al., 2016).

During most of the ice-free season, the St. Lawrence Estuary is characterized by three distinct layers: (1) a warm and salty bottom layer (LSLE, $> 150 \text{ m}$ deep, $4^\circ\text{C} < T_{\text{max}} < 6^\circ\text{C}$, $34 < S_p < 34.6$) that originates from mixing, on the continental shelf, of northwestern Atlantic and Labrador Current waters, (2) a cold intermediate layer (CIL, sitting between 50 and 150 m depth; $-1^\circ\text{C} < T_{\text{max}} < 2^\circ\text{C}$, $31.5 < S_p < 33$) that forms in the Gulf of St. Lawrence in the winter and flows landward, and (3) a warm brackish surface layer (25-50 m deep, $25 < S_p < 32$) that results from the mixture of freshwater from various tributaries (mostly the St. Lawrence and Saguenay Rivers, but also north shore rivers such as the Betsiamites, Romaine and Manicouagan) and seawater and flows seaward to ultimately form the Gaspé Current (El-Sabh and Silverberg, 1990). Seasonal variations greatly affect the surface layer, which merges with the intermediate layer during winter, as temperature and salinity change with atmospheric and buoyancy forcing, and as the contribution

from tributaries decreases during winter months (El-Sabh and Silverberg, 1990; Galbraith, 2006; Gilbert and Pettigrew, 1997).

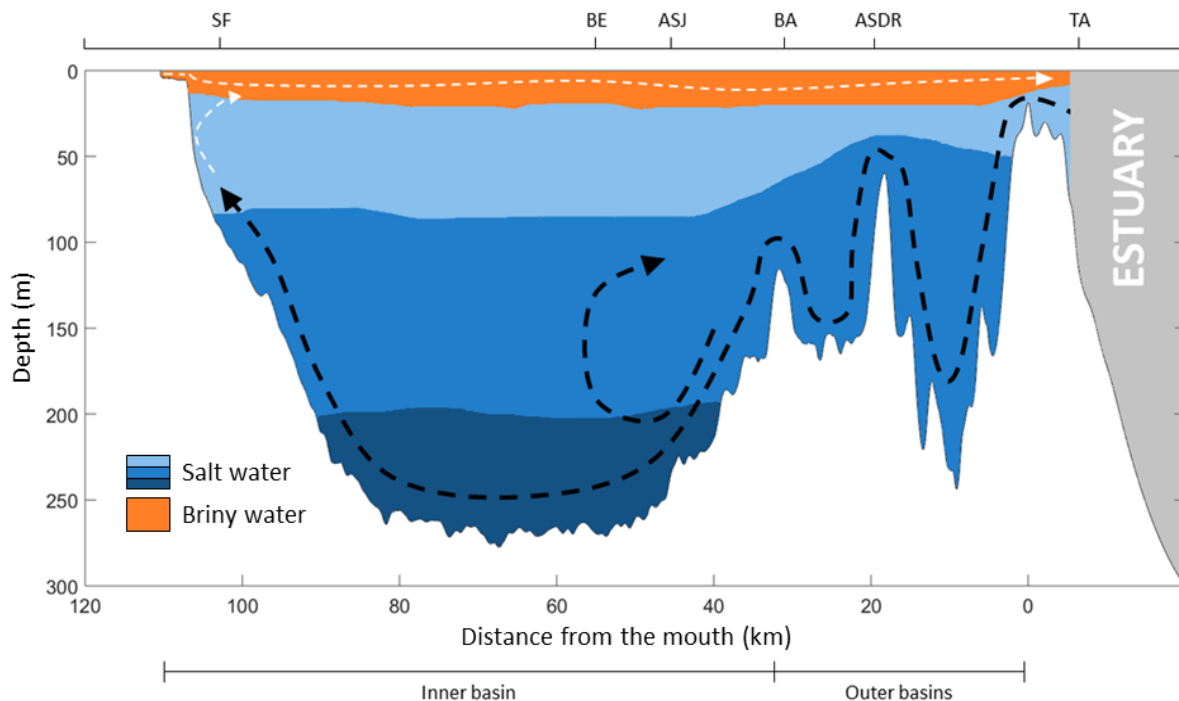


Fig. 3. Schematic representation of the Saguenay Fjord's general water circulation. White arrows illustrate the estuarine circulation, with surface current going in downstream direction. Black arrows illustrate the dense coastal inflow circulation, with deep currents going in the upstream direction. The approximate location of the following are shown: Tadoussac (TA), L'Anse de Roche (ASDR), Baie Sainte-Marguerite (BA), Anse-Saint-Jean (ASJ), Baie-Eternité (BE), St. Fulgence (SF), Baie des Ha! Ha! (BHA) (inspired from Musée du Fjord, 2002).

Likewise, the Saguenay Fjord is characterized by a strongly stratified water column that includes two main water masses: (1) a warm, shallow layer, the Saguenay Shallow Waters (SSW; 8-12 m deep, $0^{\circ}\text{C} < T < 16.8^{\circ}\text{C}$, $0.2 < S_p < 26.9$), which lies above the waters of (2) the Saguenay Deep Water (SDW; $0.9^{\circ}\text{C} < T < 4.0^{\circ}\text{C}$, $27.3 < S_p < 29.8$). Additionally, a Saguenay Intermediate Water (SIW; 20-60m deep, $2^{\circ}\text{C} < T < 3^{\circ}\text{C}$; $S \sim 30$) layer most likely forms during the summer from a mixture of surface fjord waters and the St. Lawrence Estuary Cold Intermediate Layer (CIL), when the latter spills over the entrance sill at the mouth of the fjord (Belzile et al., 2016; Bourgault et al., 2012). Nonetheless, our study shows that, because the Saguenay is a relatively

deep fjord with multiple sills, the actual vertical structure of the water column is far more complex than described above.

Belzile et al. (2016) list important distinguishing hydrographic features of the fjord, such as large vertical mixing inside the inner basin as well as important turbulence within the inner basin bottom layer. The Saguenay Fjord is seasonally ice-covered and is influenced by large tides, causing three potential renewal regimes, all dependent on the St. Lawrence Estuary dynamics (Belzile et al., 2016). These include a deep winter renewal, an intermediate summer renewal, and subsurface renewals coupled with a sudden circulation shift in the winter (Fig. 4). Water renewals are mainly due to tide movement at the entrance sill and mixing at sills, as well as within the fjord itself (Belzile et al., 2016). Internal waves of higher frequencies generated at the sill, coupled with tides, are also thought to generate turbulent mixing (Bourgault et al., 2016; Bourgault et al., 2011; Galbraith et al., 2018). Nevertheless, it is noted that environmental factors also have a noticeable impact, including wind direction (significant role in the summer), and neap-spring tide modulation (Belzile et al., 2016). Hence, summer deep renewals could be prevented by the presence of north-easterly winds, leading to freshwater piling up at the mouth of the fjord and hindering outflow from the Saguenay (Bélanger, 2003). Neap-spring tide modulation (i.e. spring tide during new and full moon, neap-tide when the sun and moon are at right angles to each other) impacts the renewal regime of the fjord, particularly on autumn-winter renewal events, with observations suggesting that they happen on a fortnightly cycle (Bélanger, 2003; Lavoie et al., 2000).

The water column stratification and circulation evolves on timescales varying from months to seasons (Belzile et al., 2016). The St. Lawrence Estuary is the source of the cold, dense water that overflows the 20 m sill, at the entrance to the fjord. The water then flows into the deep basins with flood tides on time scales estimated at only days to weeks (Bélanger, 2003). Additionally, the Saguenay Intermediate Water layer, initially driven by barotropic tidal exchange, is thought to form during the previous summer by way of the St. Lawrence Estuary Cold Intermediate Layer mixing with the fjord's surface waters, moving upward and becoming partially eroded over the winter (Bourgault et al., 2012). Furthermore, as it exchanges with particularly cold water, the new mixture resulting from the winter erosion is dense and cold

enough to sink and displace bottom waters, leading to the Saguenay Deep Water layer renewal (Bourgault et al., 2012). Thus, the Saguenay Fjord is governed by a 2-layer estuarine circulation (Fig. 3; Côté and Lacroix, 1978; Sundby and Loring, 1978).

The yellowish-brown surface waters of the fjord are characterized by high levels of dissolved organic carbon (DOC) (Tremblay and Gagné, 2009; Xie et al., 2012). Sedimentary organic matter in the Saguenay Fjord is mostly of terrestrial origin (i.e. 80%, mostly from gymnosperm vascular plants), decreasing seaward (i.e. 20-60% in the St. Lawrence Lower Estuary) (Pocklington and Leonard, 1979; St-Onge and Hillaire-Marcel, 2001; Tremblay and Gagné, 2009). Chromophoric dissolved organic matter (CDOM) was employed as a chemical tracer to identify the source of the Fjord's deep waters (Xie et al., 2012). These authors estimated that 94% by volume originates from the marine end-member (CIL) and 6% from the Saguenay River. Results of our study, presented in this thesis, also show evidence of trace amounts of the Lower St. Lawrence Estuary (LSLE) deep water in the Saguenay Fjord as well as a component of St. Lawrence River water near its mouth.

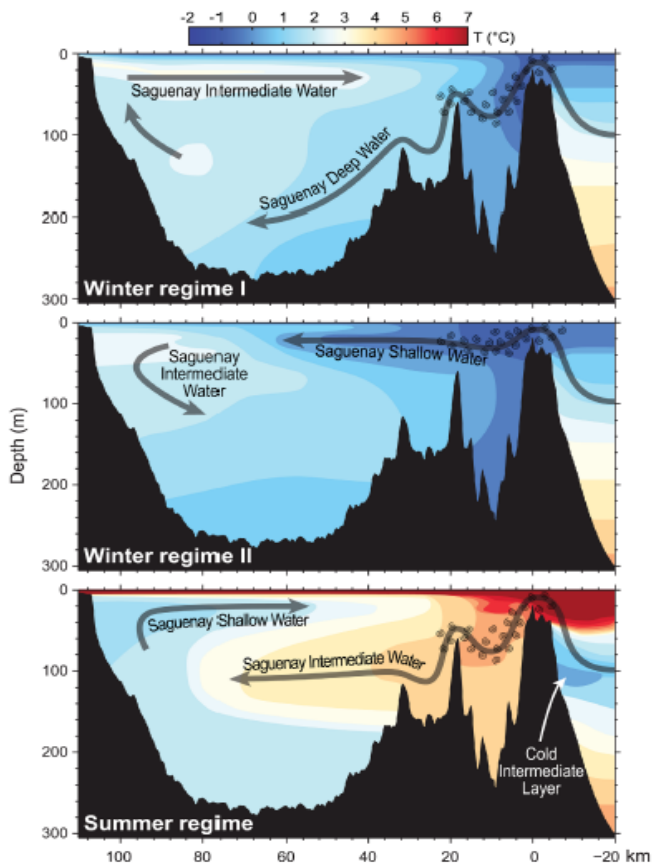


Fig. 4. Three proposed water-mass renewal regimes in the Saguenay Fjord. Top: deep winter renewal; middle: winter subsurface renewal; bottom: intermediate summer renewal (from Belzile et al., 2016).

2.3 Dominant sedimentation processes

The head of the fjord is characterized by hypopycnal sedimentation processes, with sediment accumulation rates ranging from 0.2 – 0.4 cm yr⁻¹ in the deep inner basin to 2-7 cm yr⁻¹ at the head of the fjord, near St-Fulgence (Perret et al., 1995; Smith and Walton, 1980). These rates are highly variable due to the bottom topography, as well as common mass flow events within this system (e.g., St-Jean-Vianney landslide, 1996 flood) (Mucci et al., 2015; Mucci et al., 2000; Pelletier and Lebel, 1979).

The Baie des Ha!Ha!, along with the (North) arm connecting the river and the fjord, comprise alternating layers of high organic content muds, as well as coarser quartz-rich material (Smith and Walton, 1980). The inner basin is characterized by black anoxic sandy muds (5-10%), mixing with grey muds toward the outer basins (Smith and Walton, 1980). The mouth of the fjord hosts sandy-gravels, preceded by coarse-grained sandy muds (>30%) in the outermost basin (Smith and Walton, 1980). Sedimentation rates as high as 25 cm yr⁻¹ have been reported near the head of the fjord (Syvitski et al., 1987). According to both Pocklington (1976) and Schafer et al. (1980), two sedimentation mechanisms are active at the head. Particle-by-particle deposition of riverine sediment, recharged in anthropogenic carbon waste (i.e. from pulp and paper industry), leads to sandy mud (Pocklington and Leonard, 1979). Particulate organic matter is derived from natural and anthropogenic sources but, until very recently, was thought to originate from the pulp and paper plants situated along the Saguenay River, along with terrigenous detritus (Louchouart et al., 1997; Louchouart et al., 1999; Pocklington and Leonard, 1979). Near steady-state conditions allow for the accumulation of bioturbated sediments consisting of dark grey silty clays to clayey silts on the seafloor, especially at the head of the fjord (Smith and Walton, 1980). These finer grained sediments contain 0.5% to 3% (dry weight) of organic carbon, leading to reducing conditions and hence, a thin (5mm) oxygen penetration depth (Deflandre et al., 2002; Deflandre et al., 2000; Mucci et al., 2015; Mucci et al., 2003; Mucci et al., 2000). Strain and Tan, (1979) have shown that autochthonous carbon has a negligible contribution to the sediments in the main basin, as $\delta^{13}\text{C}$ values show a narrow range of values (26.4 to -25.8‰), typical of natural terrestrial organic matter.

Phytoplankton production is considered low, as turbidity is high in the thin euphotic zone of the fjord (Therriault and Lacroix, 1975). Moreover, the physico-chemical properties of the fjord waters are unstable and thought to be unsuitable for high microalgal productivity (Chassé and Côté, 1991). Wide seasonal variations are observed, and rates of primary production in the surface waters near the head of the fjord vary between 8 and 24.5 mg-C m⁻³ h⁻¹. Primary production is dominated by the diatom *Tabellaria fenestrata*, along with two other phytoplankton species, *Asterionella Formosa* and *Melosira ambigua* (Chassé and Côté, 1991). Additionally, the high CDOM concentrations in the surface waters are also responsible for the shallowness of the euphotic zone (from 4 m to 10 m), which was observed to be thinner than the brackish surface layer although the marine waters located below are relatively clear (Côté and Lacroix, 1978). Nonetheless, the dense waters from the St. Lawrence Estuary bring relatively large amounts of particulate organic carbon, later deposited deep in the fjord (Drainville, 1968; Seibert et al., 1979; Therriault et al., 1984, 1980). Half of the dissolved organic matter (DOM) in the fjord waters is composed of humic substances, in contrast to 9-19% in the Lower St. Lawrence Estuary (Tremblay and Gagné, 2009). Dissolved organic matter concentrations decrease consistently with downstream distance and depth (i.e. toward marine conditions) (Tremblay and Gagné, 2009). Additionally, a sharp organic matter concentration gradient can be observed where freshwater loaded in DOM flows over DOM-depleted seawater (Tremblay and Gagné, 2009).

3. Impetus for estuarine research

To this day, the controversy over how, where and when organic carbon is decomposed into carbon dioxide and lost to the atmosphere throughout the coastal ocean is still debated (Cai, 2011). The magnitude of CO₂ fluxes observed in global estuaries and coastal oceans (sources of CO₂ with respect to the atmosphere) are as large as those of the continental shelves (sinks of CO₂ with respect to the atmosphere) (Fig. 5; Cai, 2011). Increasing CO₂ partial pressures (pCO₂) in the atmosphere are thought to be changing the dynamics at the air-sea interface, especially in seasonally heterotrophic shelf areas that have been observed to switch from being a CO₂ source in the preindustrial age to a CO₂ sink today. Hence, the coastal zone is likely to take up larger quantities of atmospheric CO₂ in the future as atmospheric pCO₂ increases, anthropogenic

nutrient fluxes (and primary productivity) increase, and the particulate organic carbon supply decreases in response to damming of large rivers (Cai, 2011).

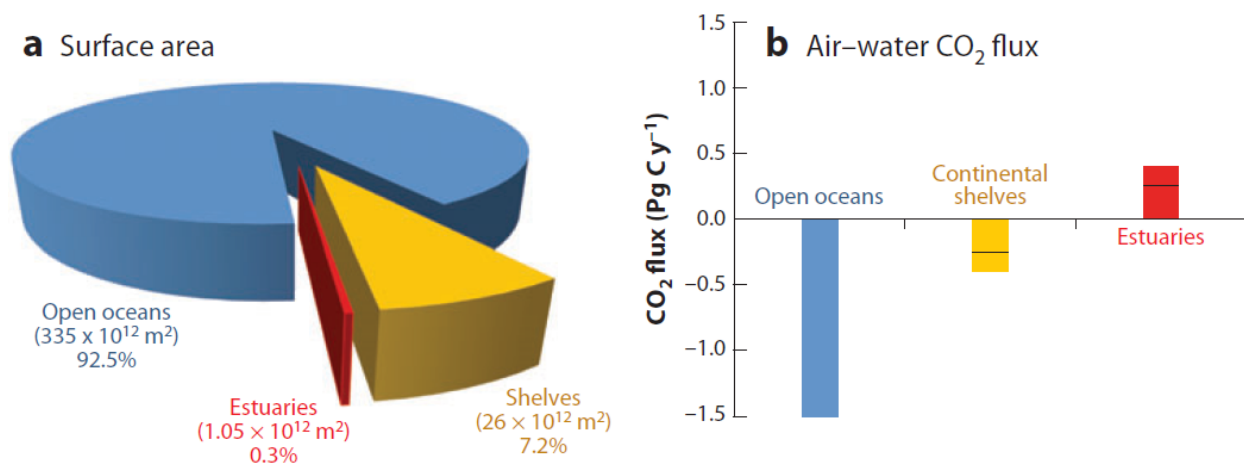


Fig. 5. a) Surface areas of estuaries, continental shelves and open oceans and **b)** their respective air-water CO₂ fluxes. From Cai (2011).

With a global, estimated efflux of $0.25 \pm 0.25 \text{ P}\cdot\text{C}\cdot\text{y}^{-1}$, estuarine waters are believed to be a significant source of CO₂ to the atmosphere (Cai, 2011). Large and fast-transit rivers carry important quantities of terrestrial organic matter and nutrients, thus contributing to respiration in ocean margins and interiors while exchanging large amounts of matter and energy with the open ocean and, thus, are one of the most biogeochemically active areas of the biosphere (Borges, 2005; Gattuso et al., 1998). Increases in atmospheric CO₂ concentration largely drive the contemporary CO₂ uptake in mid- to high-latitude continental shelves, estimated at $0.35 \text{ Pg}\cdot\text{C}\cdot\text{y}^{-1}$, and weakening of CO₂ release from lower-latitude ocean margins ($0.10 \text{ Pg}\cdot\text{C}\cdot\text{y}^{-1}$), where most riverine organic matter is normally delivered and respired (Cai, 2011). Although more attention has been paid to estuarine research over the past 15 years, there is a critical need for further investigations of estuarine and shelf CO₂ fluxes, at both various spatial and temporal scales. Better estimates of the trophic status of individual estuaries will improve the accuracy of global estuarine CO₂ fluxes and carbon budgets (Cai, 2011).

The pCO₂ in the surface waters of estuaries (pCO_{2-swe}) can easily be computed from any two of the following measurable carbonate system parameters: pH, total alkalinity (TA) and dissolved inorganic carbon (DIC) and the appropriate carbonic acid dissociation constants (Park,

1969). Currently, calculated $p\text{CO}_2$ data are considerably more abundant than directly measured values (Abril et al., 2015). Generally, $p\text{CO}_{2\text{-sw}}$ values are calculated from pH and TA, as well as water temperature and salinity. However, numerous studies have provided evidence that $p\text{CO}_{2\text{-swe}}$ values calculated from pH and TA are overestimated compared to direct measurements (Orr et al., 2018; Guérin et al., 2007; Hunt et al., 2011; Butman and Raymond, 2011). Analytical errors and uncertainties further arise from the set of dissociation constants used in the calculations of $p\text{CO}_2$ values, hence emphasizing the need for direct measurements, especially at low salinities where results differ greatly depending on the selected constants (Dinauer and Mucci, 2017; Orr et al., 2018). Substantial reduction in combined standard uncertainties can only be achieved if the standard error in the equilibrium constants, K_1 and K_2 , is better estimated, especially their pressure coefficients (Orr et al., 2018). Wang et al. (2013) also showed that the contribution of organic acid anions to TA is significant in some rivers and therefore leads to an overestimation of calculated $p\text{CO}_{2\text{-swe}}$ values. Hence, the extremely high $p\text{CO}_{2\text{-swe}}$ values, reported in some publications for low-alkalinity, high dissolved organic matter systems are potentially biased, being 50 to 300% larger than to direct, in-situ $p\text{CO}_2$ measurements (Abril et al., 2015). Given the growing interest in the role of coastal waters in the marine carbon cycle and the questionable $p\text{CO}_{2\text{-swe}}$ estimates published to date, a more stringent investigation of carbon and carbon dioxide fluxes in estuarine waters is warranted.

Fjords, which are part of the estuarine family, stand amongst the most productive ecosystems on the planet, while they have a yet unexplored role in regional and global carbon cycles (Juul-Pedersen et al., 2015). They are crucial hotspots for organic carbon (mostly terrestrial) burial and account for nearly 11% of the annual organic carbon burial flux in marine sediments, while covering only 0.12% of oceans' surface (Rysgaard et al., 2012; Smith et al., 2015). In other words, organic carbon burial rates in fjords are a hundred times faster than the average rate in the global ocean. Rates of organic carbon burial provide insights on the long-term mechanism that controls atmospheric O_2 and CO_2 concentrations over geological timescales (Smith et al., 2015). Hence, studying the carbon budget of fjord inlets not only provides information on its trophic status (i.e. source or sink of CO_2 with respect to the atmosphere) and surface-water chemistry, but also explores the magnitude of gas exchange and the amount of

biological activity it sustains. Anthropogenic activities are altering the continental water cycle, along with the flows of sediment, carbon and nutrients to the coastal oceans (Borges, 2005). Hence, the sequestration of anthropogenic CO₂ emissions by the oceans will surely be affected. Current research on CO₂ fluxes in coastal zones is still too scarce to make precise climate change prediction (i.e. flux within $\pm 0.05 \text{ Pg}\cdot\text{C}\cdot\text{y}^{-1}$) in terms of mitigating or accelerating atmospheric CO₂ levels.

The Saguenay Fjord, the southernmost subarctic fjord in the world, is an important ecosystem for the study of carbon sources and sinks. Fjords, often considered as miniature oceans, are ideal sites to study terrestrial carbon sequestration and its variation in response to climate change as carbon inputs and outputs are easily quantified in these quasi-closed marine systems. Given the looming climate crisis, fjords are valuable assets of estuarine research. This thesis characterizes, for the first time, the spatial distribution of surface-water CO₂ partial pressures ($p\text{CO}_{2\text{-SW}}$) in the Saguenay Fjord, based on a multi-year sampling of carbonate system parameters (salinity, temperature, pH, alkalinity and dissolved inorganic carbon), while outlining the general stratification of the water column in the fjord. This study therefore provides an important framework for the future study of carbon cycling in fjord waters, which play a disproportionately important – yet poorly understood – role in the global estuarine carbon cycle and climate.

4. Thesis objectives

The objectives of this thesis include:

- i. determine the relative contribution of the source-type water masses (i.e., CIL, Saguenay River and other freshwater/marine tributaries) to the water column structure in the fjord using geochemical and isotopic tracers;
- ii. reconstruct the properties of the water column (temperature, salinity, pH, pCO₂, alkalinity, nutrient concentrations), particularly the surface waters using a conservative mixing model, and further our understanding of bottom-water renewal and circulation in the Saguenay Fjord;
- iii. by comparing results of the mixing model to field measurements, identify factors, other than conservative mixing (i.e. biological activity, gas exchange), that impact the CO₂ fluxes at the air-sea interface throughout the fjord and document the trophic status of the fjord (i.e. whether it is a source of a sink of CO₂ to the atmosphere) during the study period.

The methods and results of this study are presented in the form of a manuscript destined for publication. The latter provides a detailed description of the multi-year, spatial distribution of surface-water pCO₂ throughout the fjord, a computation of CO₂ fluxes per sampling month and results of a water mixing model. The key processes controlling the CO₂ flux along the fjord are also investigated, including air-sea gas exchange and net photosynthesis/respiration. Additionally, a multi-tracer, quantitative water mass analysis that identifies the source waters involved in the deep-water renewals in the fjord is reported. Finally, concluding remarks are presented, along with suggestions for future work.

Connecting text

The following manuscript presents results of a study of the surface-water carbonate chemistry in the Saguenay Fjord and provides: 1) the relative contribution of known source-waters to the water column in the fjord, estimated from the solution of an optimization multiparameter algorithm (OMP) using geochemical and isotopic tracers, and 2) results of a conservative mixing model, based on the OMP analysis and from which theoretical surface-water $p\text{CO}_2$ values are derived and then compared to field measurements. The latter comparison serves to identify the dominant factors, other than physical mixing (i.e. biological activity, gas exchange), that impact the CO_2 fluxes at the air-sea interface throughout the fjord and reveal the trophic status of the fjord (i.e. whether it is a source or a sink of CO_2 to the atmosphere). Despite all the research done to date, the extent and frequency of water and carbon exchange between the estuary and the fjord remain unquantified. The aim of this paper is to fill yet another data gap in estuarine carbon research.

This manuscript will be submitted for publication to *Biogeosciences* or *Marine Chemistry*.

Chapter 2: Spatial variations of CO₂ fluxes in the Saguenay Fjord (Québec, Canada) and results of a water mixing model

Louise Delaigue^{1,3}, Helmuth Thomas² and Alfonso Mucci¹

¹ GEOTOP and Department of Earth and Planetary Sciences, McGill University, 3450 University Street, Montreal, QC H3A 0E8, Canada

²Department of Oceanography, Dalhousie University, Halifax, Nova Scotia, Canada

³Corresponding author (louise.delaigue@mail.mcgill.ca)

Abstract

The Saguenay Fjord is a major tributary of the St. Lawrence Estuary and is strongly stratified. A 6-8 m wedge of brackish water typically overlies up to 270 m of seawater. Relative to the St. Lawrence River, the surface waters of the Saguenay Fjord are more acidic and host lower dissolved inorganic carbon (DIC) and higher dissolved organic carbon (DOC) concentrations. The surface waters of the fjord are projected to be a net source of CO₂ to the atmosphere. Nonetheless, the intrusion, at the surface, of brackish water from the upper estuary with the rising tide, as well as mixing of seawater, overflowing the sill from the lower estuary, below the pycnocline modulate the CO₂ dynamics in the fjord. Using geochemical and isotopic tracers in combination with an optimization multiparameter algorithm (OMP), we determined the relative contribution of known source-waters to the water column in the Saguenay Fjord, including waters that originate from the Lower St. Lawrence Estuary and replenish the fjord's deep basins. These results, when combined to a conservative mixing model and compared to field measurements, serve to identify the dominant factors, other than physical mixing, such as biological activity (photosynthesis, respiration) and gas exchange at the air-water interface, that impact the water properties (e.g., pH, pCO₂, nutrient concentration) of the fjord. Results indicate that the fjord's surface waters are a net source of CO₂ to the atmosphere during periods of high freshwater discharge (e.g., spring freshet) whereas the surface waters serve as a net sink of atmospheric CO₂ when their salinity exceeds ~ 5-10.

Keywords: Carbon cycle; CO₂ flux; Coastal ocean; Estuaries; Saguenay Fjord; St. Lawrence Estuary

1. Introduction

Anthropogenic emissions of carbon dioxide (CO₂) have recently propelled atmospheric CO₂ concentrations above the 410 ppm mark, the highest concentration recorded in the past 800,000 years (Lüthi et al., 2008). The oceans, the largest CO₂ reservoir on Earth, has taken up ca. 30% of the anthropogenic CO₂ emitted to the atmosphere since the beginning of the industrial era (Brewer and Peltzer, 2009; Doney et al., 2009; Orr, 2011), mitigating the impact of this greenhouse gas on global warming. On the other hand, the uptake of CO₂ by the oceans has led to alterations of seawater carbonate chemistry and a decline in the average surface ocean pH by ~0.1 units since pre-industrial times, a phenomenon dubbed ocean acidification (Caldeira, 2005). According to the Intergovernmental Panel on Climate Change (IPCC) “business as usual” emissions scenario IS92a and general circulation models, atmospheric CO₂ levels may reach 800 ppm by 2100, lowering the pH of the surface oceans by an additional 0.3-0.4 units, at a rate that is unprecedented in the geological record (Caldeira, 2005; Hönlisch et al., 2012; Rhein et al., 2013). The growing concern about the impacts of anthropogenic CO₂ emissions calls for a meticulous quantification of organic and inorganic carbon fluxes, especially in coastal ocean ecosystems such as fjords. While much attention has recently focused on high latitude waters (e.g., Canadian Arctic), coastal, seasonally ice-covered aquatic environments such as the Saguenay Fjord have displayed comparable inter-annual and climatic sea-ice cover variabilities (Bourgault et al., 2012). Characteristics of typical Arctic coastal ecosystems are found in the Saguenay Fjord, including the presence of many species of plankton, fish, birds and marine mammals as well as important freshwater inputs and seasonal ice cover (Bourgault et al., 2012).

This study presents 1) the relative contribution of known source waters to the water column in the fjord, estimated from the solution of an optimization multiparameter algorithm (OMP) using geochemical and isotopic tracers, and 2) results of a conservative mixing model, based on results of the OMP analysis and from which theoretical surface-water pCO₂ values are derived and then compared to field measurements. The latter comparison serves to identify the dominant factors, other than physical mixing (i.e. biological activity, gas exchange), that impact

the CO₂ fluxes at the air-sea interface throughout the fjord and reveal the trophic status of the fjord (i.e. whether it is a source or a sink of CO₂ to the atmosphere).

2 Data and methods

2.1 Study site characteristics

Located in the subarctic region of Québec, eastern Canada, the Saguenay Fjord is up to 275 m deep, 110 km long and has an average width of 2 km, with a 1.1 km wide mouth where it connects to the head of the Lower St. Lawrence Estuary (Fig. 1a). The fjord's bathymetry includes three basins bound by three sills (Fig. 1b). The first one, at a depth of ~20 m, is located at its mouth near Tadoussac and controls the overall dynamics of the fjord. The second is located 18 km further upstream and sits at a depth of 60m, while the third one is found another 32 km upstream and rises to a depth of 115 m. The fjord's drainage basin is 78,000 km² and is part of the greater St. Lawrence drainage basin (Smith and Walton, 1980), forming a hydrographic system, along with the Great Lakes, of more than 1.36 million km².

Tributaries to the Saguenay Fjord include the Saguenay, Éternité and Sainte-Marguerite Rivers (Fig. 1b). The Saguenay River is the main outlet from the Saint-Jean Lake, and flows into the North Arm of the fjord near St. Fulgence (Fig. 1b) with a mean freshwater discharge of ~1200 m³ s⁻¹ (Bélanger, 2003). Two other local, minor tributaries, the Rivière-à-Mars (95 km long, mean discharge ~8 m³ s⁻¹) and the Rivière Ha! Ha! (35 km long, mean discharge ~15 m³ s⁻¹) discharge into the Baie des Ha! Ha!, a distinct feature of the Saguenay Fjord. Finally, the fjord receives denser marine waters from the St. Lawrence Estuary, filling the three basins, as these waters episodically overflow the entrance sill (Therriault and Lacroix, 1975; Stacey and Gratton, 2001; Bélanger, 2003; Belzile et al., 2016).

The overflow and the intrusion of marine waters from the St. Lawrence Estuary generate a sharp halocline, leading to a simplified description of the water stratification in the fjord (Fig 1.b): a thin brackish surface layer (5-10 m, $S_p \sim 10$ where S_p stands for the practical salinity) overlying a denser layer ($S_p \sim 30$) of marine waters (Belzile et al., 2016). The tidally-modulated intrusion of marine waters from the St. Lawrence Estuary into the Saguenay Fjord, as well as the

outflow of the fjord into the estuary, have a major influence on the water column stratification and circulation in the Saguenay Fjord and at its mouth. In other words, the properties of the uppermost 100 m of the water column in the adjacent estuary are critical in determining the water stratification in the Saguenay Fjord, since salinity and temperature control the density of waters that spill over the sill and fill the fjord's deep basins (Belzile et al., 2016).

During most of the ice-free season, the St. Lawrence Estuary is characterized by three distinct layers: (1) a relatively warm and salty bottom layer (LSLE, $4^{\circ}\text{C} < T_{\text{max}} < 6^{\circ}\text{C}$, $34 < S_p < 34.6$) that originates from mixing, on the continental shelf, of northwestern Atlantic and Labrador Current waters, (2) a cold intermediate layer (CIL, 150 m deep; $-1^{\circ}\text{C} < T_{\text{max}} < 2^{\circ}\text{C}$, $31.5 < S_p < 33$) that forms in the Gulf of St. Lawrence in the winter and flows landward, and (3) a warm brackish surface layer (25-50 m deep, $25 < S_p < 32$) that results from the mixture of freshwater from various tributaries (mostly the St. Lawrence and Saguenay Rivers, but also north shore rivers such as the Betsiamites, Romaine and Manicouagan) and seawater and flows seaward to ultimately form the Gaspé Current (Dickie and Trites, 1983; El-Sabh and Silverberg, 1990; Gilbert and Pettigrew, 1997). Seasonal variations greatly affect the properties of the surface layer, which merges with the intermediate layer during winter, as temperature and salinity change with atmospheric and buoyancy forcing, and the contribution from tributaries decreases during winter months (Galbraith, 2006).

Likewise, the Saguenay Fjord is characterized by a strongly stratified water column that includes at least two water masses: (1) a warm, shallow layer, the Saguenay Shallow Waters (SSW; $0^{\circ}\text{C} < T < 16.8^{\circ}\text{C}$, $0.2 < S_p < 26.9$), which lies above the waters of (2) the Saguenay Deep Water (SDW; $0.9^{\circ}\text{C} < T < 4.0^{\circ}\text{C}$, $27.3 < S_p < 29.8$). The SDW most likely forms from a mixture of surface fjord water, St. Lawrence River waters and the St. Lawrence Estuary Cold Intermediate Layer (CIL), when the latter spills over the entrance sill at the mouth of the fjord (Bourgault et al., 2012; Belzile et al., 2016). Nonetheless, our study shows that, because the Saguenay Fjord is a relatively deep fjord with multiple sills, the actual vertical structure of the water column is far more complex than described above.

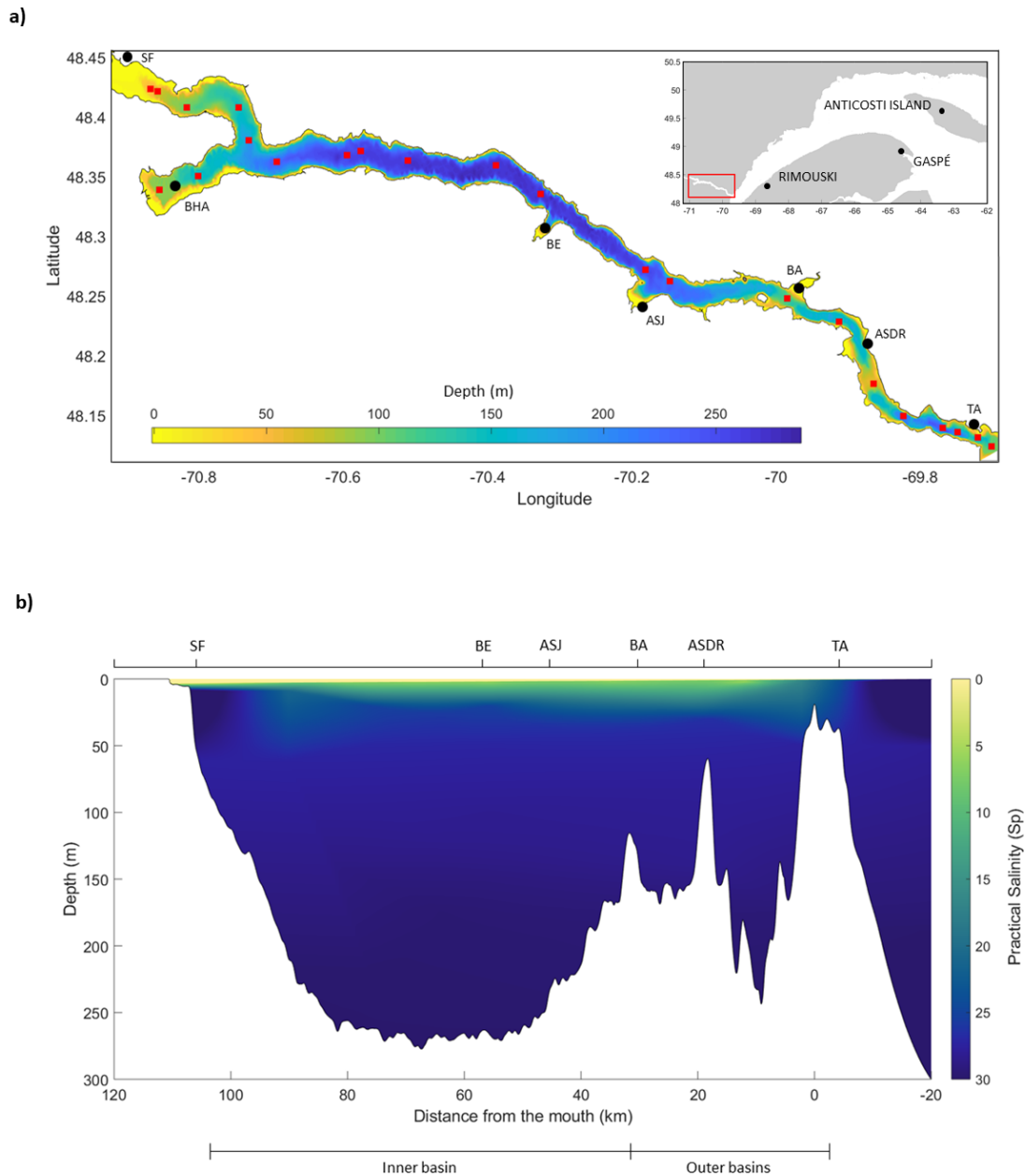


Fig. 1 a) Bathymetry and geographic location of the Saguenay Fjord. Red dots represent the hydrographic stations sampled in the Saguenay Fjord during R/V Coriolis II cruises. **b)** Longitudinal section of the Saguenay Fjord, showing the strong halocline. The approximate location of the following are shown: Tadoussac (TA), L'Anse de Roche (ASDR), Baie Sainte-Marguerite (BA), Anse-Saint-Jean (ASJ), Baie-Eternité (BE), St. Fulgence (SF), Baie des Ha! Ha! (BHA).

2.2 Water-column sampling

The data presented in this paper were gathered during the ice-free season on four cruises, between the years 2014 and 2017 aboard the R/V Coriolis II, in late spring (May 2016) and early summer (June 2017), as well as early and late fall (September 2014, November 2017). Sampling of the water column was carried out with a rosette system along the central axis of the Saguenay Fjord, between St. Fulgence and the mouth of the Fjord, including the Baie des Ha! Ha!. Stations in the St. Lawrence Estuary, near the mouth of the Fjord, were also sampled. The sampling locations are identified in Fig. 1a. The surface water of the Saguenay River was sampled with a rope and bucket in 2013 and 2017 from the Dubuc Bridge that joins Chicoutimi and Chicoutimi-Nord over the Saguenay River, to determine the chemical characteristics of the freshwater Saguenay River end-member.

The rosette system (12 x 12-L Niskin bottles) was equipped with a Seabird 911Plus conductivity-temperature-depth (CTD) probe, a Seabird® SEB-43 oxygen probe, a WETLabs® C-Star transmissometer and a Seapoint® fluorometer. The Niskin bottles were closed at discrete depths as the rosette was raised from the bottom, typically at the surface (2-3 m), 25 m, 50 m, 75 m, 100 m, and at 50 m intervals to the bottom (or within 10 m of the bottom). Samples were taken directly from the bottles for dissolved oxygen (DO), $\text{pH}_{(\text{NBS})}$ and/or $\text{pH}_{(\text{total})}$, total alkalinity (TA), dissolved inorganic carbon (DIC), dissolved silicate (DSi), practical salinity (S_P), and the stable oxygen isotopic composition of the water ($\delta^{18}\text{O}_{\text{water}}$). Water samples destined for pH measurements were transferred to 125 mL plastic bottles without headspace whereas TA and TA/DIC samples were stored in, respectively, 250 mL and 500 mL glass bottles. TA and TA/DIC samples were poisoned with a few crystals of mercuric chloride (HgCl_2) and bottles were sealed using a ground-glass stopper and Apiezon® Type-M high-vacuum grease. $\delta^{18}\text{O}_{\text{water}}$ and S_P samples were stored in 13 mL plastic screw-cap test tubes.

2.3 Analytical procedures

T and S_p were determined *in-situ* using the CTD probe. The conductivity probe was calibrated by the manufacturer over the winter prior to the cruise. In addition, the S_p of surface waters was determined by argentimetric titration at McGill University and calibration of the AgNO_3 titrant with IAPSO standard seawater. The reproducibility of these measurements is typically better than $\pm 0.5\%$.

pH_T was determined spectrophotometrically on board, on the total hydrogen ion concentration scale for saline waters ($S_p > 5$), using phenol red and purified *m*-cresol purple as indicators and a Hewlett-Packard UV-visible diode array spectrophotometer (HP-8453A) with a 5-cm quartz cell, after thermal equilibration of the sample in a constant temperature bath at 25 ± 0.1 °C. The salinity-dependence of the dissociation constants and molar absorptivities of the indicators were taken from Robert-Baldo et al. (1985) for phenol red and from Clayton and Byrne (1993) for *m*-cresol purple. The salinity-dependence of the phenol red indicator dissociation constant and molar absorptivities was extended (from $S_p = 5$ to 35; Bellis, 2002) to encompass the range of salinities encountered in this study, but computed pH_T values from the revised fit were not significantly different from those obtained with the relationship provided by Robert-Baldo et al. (1985). Results computed from these parameters yielded results that were more similar to each other as well as to potentiometric glass electrode measurements than the revised equation for the purified *m*-cresol purple provided by Douglas and Byrne (2017). The pH of low-salinity waters ($S_p < 5$) was determined potentiometrically on board at 25°C, on the NIST (formerly NBS) scale (pH_{NIST}), using a Radiometer Analytical® (GK2401C) combination glass electrode connected to a Radiometer Analytical® pH/millivoltmeter (PHM84). A calibration of the electrode was completed prior to and after each measurement, using three NIST-traceable buffer solutions: pH-4.00, pH-7.00 and pH-10.00, at 25°C. The Nernstian slope was then obtained by least-squares fitting of the electrode response to the buffer values. For waters with S_p comprised between 5 and 35, pH_{NBS} was converted to pH_T according to the electrode response to TRIS buffer solutions prepared at $S_p = 5, 15, 25$ and 35 and for which the pH_T was assigned at 25°C (Millero,

1986). Reproducibility of pH measurements, based on replicate analyses of the same sample or at least two of the three methods used was typically better than ± 0.005 .

DO concentrations were determined on board by Winkler titration on distinct water samples recovered directly from the Niskin bottles, following the method described by Grasshoff et al. (1999). The relative standard deviation, based on replicate analyses of samples recovered from the same Niskin bottle, was 0.5 %. These measurements served to calibrate the SBE-43 oxygen probe mounted on the rosette sampler.

The stable oxygen isotopic composition of the water samples ($\delta^{18}\text{O}_{\text{water}}$) was determined using the CO_2 equilibration method of Epstein and Mayeda (1953). Aliquots (200- μL) of the water samples and three laboratory internal reference waters were transferred into 3-mL vials stoppered with a septum cap. The vials were then placed in a heated rack maintained at 40°C. Commercially available CO_2 gas was introduced in all the vials using a Micromass AquaPrep and allowed to equilibrate for 7 hours. The headspace CO_2 was then sampled by the Micromass AquaPrep, dried on a -80°C water trap, and analyzed on a Micromass Isoprime universal triple collector isotope ratio mass spectrometer in dual inlet mode at the GEOTOP-UQAM Stable Isotope Laboratory. Data were normalized against the three internal reference waters, themselves calibrated against Vienna Standard Mean Ocean Water (V-SMOW) and Vienna Standard Arctic Precipitation (V-SLAP). The results are reported on the δ -scale in ‰ relative to V-SMOW:

$$\delta^{18}\text{O} = \left(\frac{(^{18}\text{O}/^{16}\text{O})_{\text{sample}}}{(^{18}\text{O}/^{16}\text{O})_{\text{VSMOW}}} - 1 \right) \times 1000 \quad (1)$$

Based on replicate analyses of the samples, the average standard deviation of the measurements was better than 0.05‰.

TA was measured using an automated Radiometer (TitraLab865[®]) potentiometric titrator and a Red Rod[®] combination pH electrode (pHC2001) at McGill University. The dilute HCl titrant was calibrated prior, during and after each titration session using certified reference materials (CRM) provided by Andrew Dickson (Scripps Institution of Oceanography). Raw titration data were processed with a proprietary algorithm designed for shallow end-point detection. Surface

water samples from the Saguenay Fjord and the Upper St. Lawrence Estuary were also analyzed at Dalhousie University using a VINDTA 3C[®] (Versatile Instrument for the Determination of Titration Alkalinity, by Marianda) following the method described in Dickson et al. (2007). A calibration of the instrument was performed against CRMs and the reproducibility of the measurements was better than 0.1%.

The DIC concentration of samples, recovered in 2016 and 2017 in the Saguenay Fjord and surface waters of the Upper and Lower St-Lawrence Estuary, were determined at Dalhousie University using the VINDTA 3C[®]. In 2014, DIC was determined on board using a SciTech Apollo DIC analyzer. Once thermally equilibrated at 25°C, 1-1.5 mL of the sample was acidified with 10% H₃PO₄ after being injected into the instrument's reactor. The evolved CO₂ was carried to a LI-COR infrared analyzer by a stream of pure nitrogen. A calibration curve was constructed using gravimetrically prepared Na₂CO₃ solutions, and the accuracy of the measurements was verified using a CRM. Reproducibility was typically on the order of 0.2%.

2.4 Calculations

2.4.1 Water mass distribution analysis

A combination of transport processes associated with ocean circulation and biogeochemical cycles generally controls the distribution of tracers in the ocean (Chester, 1990). Resolving the effects of mixing and biogeochemical cycling is imperative if one is to evaluate the movement of nutrients and tracers in a water body. An Optimum Multi-Parameter (OMP) analysis allows for the determination of the relative contributions of pre-defined source-water types (SWT) representing the parameter values of the unmixed water masses in one specific geographic location, by optimizing the hydrographic data gathered in a given system (Tomczak, 1981). The original OMP algorithm is a linear inverse model that assumes all hydrographic tracers are conservative. The algorithm has since been modified to handle non-conservative properties such as DIC and nutrients by taking into consideration the stoichiometry of microbial respiration and photosynthesis (Dinauer and Mucci, 2018; Karstensen and Tomczak, 1998).

OMP calculates the SWT fractions x_i for each data point by finding the best linear mixing combination defined by parameters such as temperature, salinity, $\delta^{18}\text{O}_{\text{water}}$, TA, and DIC. The contributions from all SWT must add-up to 100% and cannot be negative. Assuming that four SWT (a, b, c, and d) are sufficient to characterize the water column structure, and five parameters (T, S, $\delta^{18}\text{O}_{\text{water}}$, TA, and DIC) characterize each of these, the following set of linear equations is solved in the classical OMP analysis (MATLAB - version 1.2.0.0; Karstensen, 2013):

$$x_a T_a + x_b T_b + x_c T_c + x_d T_d = T_{obs} + R_T \quad (2a)$$

$$x_a S_a + x_b S_b + x_c S_c + x_d S_d = S_{obs} + R_S \quad (2b)$$

$$x_a \delta^{18}O_a + x_b \delta^{18}O_b + x_c \delta^{18}O_c + x_d \delta^{18}O_d = \delta^{18}O_{obs} + R_{\delta^{18}O} \quad (2c)$$

$$x_a TA_a + x_b TA_b + x_c TA_c + x_d TA_d = TA_{obs} + R_{TA} \quad (2d)$$

$$x_a DIC_a + x_b DIC_b + x_c DIC_c + x_d DIC_d = DIC_{obs} + R_{DIC} \quad (2e)$$

$$x_a + x_b + x_c + x_d = 1 + R_{\Sigma} \quad (2f)$$

where T_{obs} , S_{obs} , $\delta^{18}O_{obs}$, TA_{obs} , and DIC_{obs} are the observed values in any given parcel of water and R are their associated fitting residuals. T_i , S_i , $\delta^{18}O_i$, TA_i , and DIC_i ($i = a, \dots, d$) are the characteristic values of each SWT (Lansard et al., 2012; Tomczak and Large, 1989; Mackas et al., 1987). Mass conservation is expressed in Equation 2f.

To account for potential environmental variability, measurement inaccuracies, and allow for the comparison of parameters with incommensurable units, a weighting procedure based on covariances between tracers is applied. In this study, weights were assigned arbitrarily based on their conservative behaviors and variability (Lansard et al., 2012). Conservative tracers (i.e. S_p , TA, $\delta^{18}O$) were appointed heavy weights, while non-conservative tracers (i.e. T, DO, DIC) were given low weights according to their seasonal variability. For instance, temperature in the surface waters of the Saguenay River ranges from 3.1°C in the winter to 21°C in the summer. Dissolved oxygen was also considered as a non-conservative tracer as it is heavily reliant on temperature and salinity, as well as biological activity. DIC was given an intermediate weight given that it is

relatively conservative except in the surface waters, where photosynthesis and air-sea gas exchange take place.

2.4.2 Source-Water Type definitions

A water mass is, by definition, a body of water having its origin in a particular source region (Tomczak, 1999). An OMP analysis requires the user to define the major water masses contributing to the structure of the water column in the study area. In the context of biogeochemical cycles, a SWT should be defined where the water mass enters the basin, upstream from the mixing region (Karstensen, 2013). Parameter values are preferably extrapolated from hydrographic observations in the water mass formation regions or can be found in the literature.

In this study, source-water type definitions were derived from property-property diagrams (See Annex, Fig. A) of an observational dataset relevant to the Saguenay Fjord: the Saguenay River (SWR), the St. Lawrence Estuary summertime Cold Intermediate Layer (CIL), the Lower St. Lawrence Estuary bottom waters (LSLE) and the St. Lawrence River (SLRW). Each definition was captured relative to the fjord, i.e. each source-water type is only appropriate for the fjord and for the period of study. Definitions and weights are reported in Table 1.

SWT	Salinity (S_p)	Temperature (°C)	TA _(meas) ($\mu\text{mol.kg}^{-1}$)	$\delta^{18}\text{O}$ (‰)	DIC ($\mu\text{mol.kg}^{-1}$)	DO ($\mu\text{mol.kg}^{-1}$)
SRW	0.00 ± 0	6.19 ± 0.18	154 ± 13	-12.17 ± 0.21	230 ± 12	411 ± 6
CIL	32.52 ± 0.05	1.44 ± 0.08	2210 ± 2	-1.12 ± 0.03	2141 ± 3	256 ± 5
LSLE	34.31 ± 0.01	5.16 ± 0.18	2294 ± 2	-0.17 ± 0.02	2276 ± 3	76 ± 1
SLRW	0.00 ± 0	12.11 ± 0.13	1099 ± 16	-8.09 ± 0.13	1140 ± 15	329 ± 5
Weights	25	1	25	25	15	1

Table 1. Source-Water Type (SWT) definitions for the Saguenay River (SWR), the St. Lawrence Estuary summertime Cold Intermediate Layer (CIL), the Lower St. Lawrence Estuary bottom water (LSLE) and the St. Lawrence River (SLRW). Definitions were derived from data taken in September 2014, May 2016, June 2017 and November 2017. Data for SRW and SLRW were extrapolated to $S_p = 0$. The weights used in the OMP analysis are also shown.

2.4.3 CO₂ partial pressures

The CO₂ partial pressure in seawater ($p\text{CO}_{2(\text{SW})}$) is defined as the $p\text{CO}_2$ in water-saturated air ($p\text{CO}_{2(\text{air})}$) in equilibrium with the water sample or the ratio of the CO₂ concentration in solution to the equilibrium concentration at T, P and S_p , multiplied by the actual $p\text{CO}_{2(\text{air})}$. As direct measurements of the surface mixed layer $p\text{CO}_2$ were not available, it was calculated using CO2SYS (Excel v2.1; Denis Pierrot of NOAA, 2006) and the measured pH (total or NBS scale), DIC ($\mu\text{mol.kg}^{-1}$), in-situ temperature ($^{\circ}\text{C}$), practical salinity (S_p) and pressure (dbar) as input parameters. When available, soluble reactive phosphate (SRP) and dissolved silicate (DSi) concentrations were also included in the calculations, but their inclusion did not affect the results significantly because their concentrations are relatively low in surface waters (0.49 μM and 37.0 μM , respectively) and introduce an insignificant error. DIC, rather than TA was used as an input parameter to CO2SYS since the fjord surface waters are enriched in colored dissolved organic carbon (> 4 mg/L), delivered by the Saguenay River, and are characterized by a negative organic alkalinity (positive organic acidity). The carbonic acid dissociation constants (K^*_1 and K^*_2) of Cai and Wang (1998) were used for the calculations, as the latter are more suitable for the low-salinity conditions encountered in estuarine environments such as the Saguenay Fjord ($S_p < 20$) (Dinauer and Mucci, 2017). $p\text{CO}_{2(\text{SW})}$ values were computed for the surface mixed layer located above the sharp pycnocline (~10 m) where most physical and chemical properties are directly impacted by biological activity (photosynthesis and respiration) as well as heat and gas exchange across the air-sea interface (Table 2). $p\text{CO}_{2(\text{SW})}$ were normalized ($p\text{CO}_{2(\text{SST})}$) to the average surface water temperature per sampling month (i.e. $T = 10.4^{\circ}\text{C}$ for September 2014, $T = 5.04^{\circ}\text{C}$ for May 2016, $T = 11.9^{\circ}\text{C}$ for June 2017, and $T = 7.13^{\circ}\text{C}$ for November 2017), per station, to account for the effects of temperature on the CO₂ solubility in water following the procedure described in Jiang et al. (2008).

The surface waters of the fjord are generally a net source of CO₂ to the atmosphere (Fig. 4, Table 3). Yet, the fjord appeared to be a net sink of atmospheric CO₂ in September 2014 and a net source of CO₂ to the atmosphere in May 2016. Since most of the available data were gathered

in the spring, additional samplings and analyses were carried out in November 2017, following the methodologies described in sections 2.1 and 2.2.

2.4.4 CO₂ flux across the air-sea interface

The difference between the air and sea-surface pCO₂ values ($\Delta pCO_2 = pCO_{2(sw)} - pCO_{2(air)}$) determines the direction of gas exchange and whether the surface mixed layer of a body of water is a source or a sink of CO₂ for the atmosphere. The air-sea CO₂ gas exchange, or CO₂ flux, can be estimated at each station using the following relationship:

$$FCO_2 = k \cdot K_0 \cdot (\Delta pCO_2) \quad (3a)$$

where F is the flux of CO₂ across the air-sea interface in mmol·m⁻²·d⁻¹, k is the gas transfer velocity of CO₂ in cm h⁻¹ (Wanninkhof, 1992), K_0 is the solubility coefficient of CO₂ in mol·kg⁻¹·atm⁻¹ at the *in-situ* temperature and salinity of the surface waters (Weiss, 1974), and ΔpCO_2 is the difference between the air and sea-surface pCO₂ values in μ atm. Positive values of F indicate the release of CO₂ to the atmosphere by surface waters, whereas negative values imply that surface waters serve as a sink of CO₂. The flux of CO₂ was computed for each sampling month, using the pCO_{2(air)} for each sampling date (395 μ atm for September 2014, and 407 μ atm for May 2016, and 408 μ atm June and November 2017).

The gas transfer velocity of CO₂ was calculated using the revised relationship of Wanninkhof (2014):

$$k = 0.215u^2 (Sc/660)^{-1/2} \quad (3b)$$

where u is the wind speed (m s⁻¹) and Sc is the Schmidt number (Wanninkhof, 2014). Wind speed was estimated using the hourly station wind speed data from Environment Canada at the La Baie weather observing station, for each sampling month. The Schmidt number is defined as the kinematic viscosity of water divided by the diffusion coefficient of CO₂. Sc was corrected for the temperature dependence of CO₂ in freshwater ($S_p = 0$), assuming that k is proportional to $Sc^{-1/2}$ (Wanninkhof, 1992). In the case of CO₂, the increase in $Sc^{-1/2}$ (and therefore k) with increasing temperature is compensated for by a decrease in solubility, therefore k was considered nearly temperature independent (Wanninkhof, 1992). Sc was computed using:

$$Sc = A + Bt + Ct^2 + Dt^3 + Et^4 \quad (3c)$$

where t is the temperature (degrees Celcius) and A, B, C, D and E are fitting coefficients for seawater ($S_p = 35$) and freshwater ($S_p = 0$), for temperatures ranging from -2°C to 40°C (Wanninkhof, 2014). The uncertainty in Sc ranges from 3 to 10%, and is mainly due to the diffusion coefficients (Wanninkhof, 2014). Estimates of k , calculated at each sampling point using the equation from Wanninkhof (2014), ranged from 0.36 to 3.37 cm h^{-1} for the fjord, compared to 1.6 to 4.5 cm h^{-1} in the St. Lawrence Estuary (Dinauer and Mucci, 2017).

Atmospheric $p\text{CO}_2$ data ($p\text{CO}_{2(\text{air})}$) were computed using the daily averages of measured mole fractions of CO_2 in dry air, obtained at the La Baie weather station and retrieved from the Climate Research Division at Environment and Climate Change Canada. The mean $p\text{CO}_{2(\text{air})}$ was then calculated for each year using the following equation:

$$p\text{CO}_{2(\text{air})} = x\text{CO}_2 \cdot (P_b - P_w) \quad (4)$$

where $x\text{CO}_2$ is the measured mole fraction of CO_2 in dry air in ppm, P_b is the barometric pressure at the sea surface in atm, and P_w is the saturation water vapor pressure at in-situ temperature and salinity, in atm. P_b was obtained using the conversion formula of Tim Brice and Todd Hall (from NOAA's National Weather Service), using the La Baie weather station's elevation. P_w was calculated using the Rivière-à-Mars properties (i.e. closest body of water to the weather station) and the P_w calculated from its relationship to T and S_p provided by Weiss and Price (1980).

The fjord was divided into two segments, one including the inner basin and the other encompassing the two outer basins, as each segment often displays distinct behaviors. Thus, the area-averaged CO_2 flux ($F_{\text{area-avg}}$) was computed individually for both segments, as well as the fjord as a whole, following the procedure described by Jiang et al. (2008):

$$F_{\text{area-avg}} = \frac{\sum F_i \times S_i}{\sum S_i} \quad (5)$$

where F_i is the average of all the fluxes within segment i , and S_i is the surface area of segment i . The fjord's surface area (319.3 km^2) was computed in MATLAB, using a land mask acquired from Fisheries and Oceans Canada.

2.4.5 Water Mixing Model

A two end-member mixing model was constructed based on the chemical properties of the freshwater delivered to the fjord (Saguenay River) and marine bottom waters entering the fjord from the St. Lawrence Estuary (Fig. 2a). As shown in the results of the OMP analysis (section 3.1), the LSLE and SLRW were shown to have a negligible influence on the fjord's water structure, and thus were not included in the model. In fact, given that the carbonate chemistries of the CIL and LSLE waters are similar, the bottom waters were assumed to be well mixed and constitute a single end-member. This is illustrated in Fig. 2, as the high S_p end-member alkalinity extends linearly beyond that of the CIL end-member (Table 1). The measured surface TA were strongly correlated to S_p ($R^2 = 0.99$) in the fjord waters. Therefore, end-member properties were obtained by extrapolating the surface water (above the pycnocline) data to $S_p = 0$ and bottom-water data to the highest measured salinity (Fig. 2a). The organic alkalinity of the fjord waters was estimated from the difference between the measured and calculated TA ($TA_{(calc)}$; Fig. 2b). The latter was calculated using CO2SYS (Excel v2.1; Denis Pierrot of NOAA) and pH and DIC as input parameters. The end-member source waters were then mixed, assuming that $TA_{(calc)}$ and DIC behave conservatively.

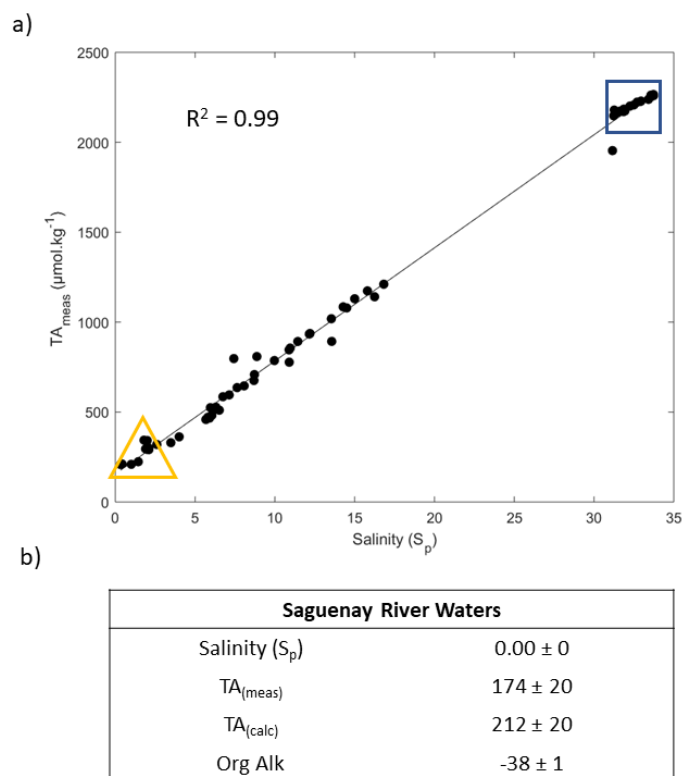


Fig. 2 a) Salinity (S_p) versus measured alkalinity ($TA_{(meas)}$) for SRW and CIL data points, for all sampling months ($R^2 = 0.99$). The yellow triangle defines the properties of the SRW, and the dark blue square comprises the properties of the CIL. **b)** $TA_{(meas)}$, $TA_{(calc)}$ and Org Alk definitions for the Saguenay River (SRW), using surface data from all sampling months, with standard error. The Org Alk (positive) contribution to the TA of the CIL is not considered as it accounts for less than 0.1 % of its TA.

Hence, the salinity, total alkalinity ($TA_{(mix)}$) and dissolved inorganic carbon ($DIC_{(mix)}$) of the mixed solutions were calculated using the following equations:

$$S_{P(mix)} = \frac{m_1 S_{P1} + m_2 S_{P2}}{(m_1 + m_2)} \quad (6a)$$

$$TA_{(mix)} = \frac{m_1 TA_{(calc\ 1)} + m_2 TA_{(calc\ 2)}}{(m_1 + m_2)} \quad (6b)$$

$$DIC_{(mix)} = \frac{m_1 DIC_1 + m_2 DIC_2}{(m_1 + m_2)} \quad (6c)$$

where m_i are the mass contributions of each end-member to the mixture.

$pCO_{2(sw-mix)}$ was then calculated from $TA_{(mix)}$ and $DIC_{(mix)}$ for salinities ranging from 0 to 33, at four different temperatures (0°C, 5°C, 10°C and 15°C) using CO2SYS. Results of the model (Fig. 7) show that at the lower and higher salinities, the $pCO_{2(sw-mix)}$ is elevated, and the fjord serves as a source of CO_2 to the atmosphere, but at intermediate salinities ($5 < S_P < 15$) or mixing ratios, the fjord may serve as a sink of atmospheric CO_2 when surface water temperatures are close to freezing. The data from the various cruises are superimposed on the model results, after correction for the organic alkalinity.

2.4.6 Salinity normalization of DIC in surface waters

To quantitatively evaluate the impact of biological activity on the DIC budget in the surface waters of the fjord, DIC and $TA_{(calc)}$ were normalized to the average surface salinity of each sampling month ($S_P = 11.7$ for September 2014, $S_P = 2.58$ for May 2016, $S_P = 7.61$ for June 2017 and $S_P = 10.9$ for November 2017) following the procedure of Friis *et al.* (2003):

$$NDIC = \frac{DIC^{meas} - DIC^{S=0}}{S^{meas}} \cdot S^{ref} + DIC^{S=0} \quad (7)$$

where DIC^{meas} is the measured DIC, $DIC^{S=0}$ is the DIC extrapolated to $S_P = 0$, S^{meas} is the measured salinity and S^{ref} is the average measured salinity per sampling month (Friis *et al.*, 2003). The change in NDIC (i.e. $\Delta NDIC$) along the fjord, relative to the waters at the head of the fjord, was then computed for each sampling month and results can be found in Fig. 9. These

values reveal how DIC evolves along the fjord beyond what is expected based on conservative mixing.

2.4.7 Oxygen saturation and apparent oxygen utilization in the surface waters

To further account for the biological activity in the surface waters, the degree of oxygen saturation was calculated for each sampling month in the surface waters of the fjord using:

$$\% \text{ sat} = ([O_2]_{meas} / [O_2]_{equil}) \times 100 \quad (8)$$

where $[O_2]_{meas}$ is the dissolved oxygen content measured in the fjord waters, and $[O_2]_{equil}$ is the equilibrium dissolved oxygen concentration (or solubility) at *in-situ* conditions (i.e. temperature and salinity) for each sample.

The oxygen saturation indicates if the system is either autotrophic (i.e. production of oxygen, dominated by photosynthesis) or heterotrophic (consumption of oxygen, dominated by microbial respiration). The oxygen saturation remains a qualitative proxy as O_2 exchange at the air-sea interface is about 9 times faster than CO_2 exchange (Zeebe and Wolf-Gladrow, 2001). The apparent oxygen utilization (AOU) was also computed from the difference between $[O_2]_{equil}$ and $[O_2]_{meas}$.

3 Results and discussion

3.1 Water mass analysis

Relative contributions (mixing ratios, f) of the Saguenay River (SRW), Cold Intermediate Layer (CIL) from the St. Lawrence Estuary and Lower St. Lawrence Estuary (LSLE) bottom waters throughout the Saguenay Fjord's water column for the sampling month of June 2017 are shown in Fig. 3. As expected, the SRW and CIL are dominant contributors, with the SRW forming a brackish surface layer ($f = 1$ in surface waters), and the CIL replenishing the bottom waters of the fjord ($0.7 < f < 1$). According to the OMP analysis, the LSLE have a small contribution to the bottom waters ($f = 0.2$), adding to the complexity of the water structure. Although somewhat unexpected, this can readily be explained by tidal upwelling, internal waves and intense turbulent

mixing of the water column at the head of the Laurentian Channel (Gratton et al., 1988; Saucier and Chassé, 2000). The relative contribution of the LSLE in the deep waters of the fjord is small and could only be detected because of the suite of geochemical and isotopic tracers used in the OMP analysis, especially the difference in the $\delta^{18}\text{O}$ signature of the CIL and LSLE. The contribution from the St. Lawrence River Water (SLRW) is negligible as it intrudes slightly at the surface at the mouth of the fjord and is thus not shown here.

Although the water column structure is similar throughout the year, seasonal variations do occur and will be addressed in a forthcoming paper.

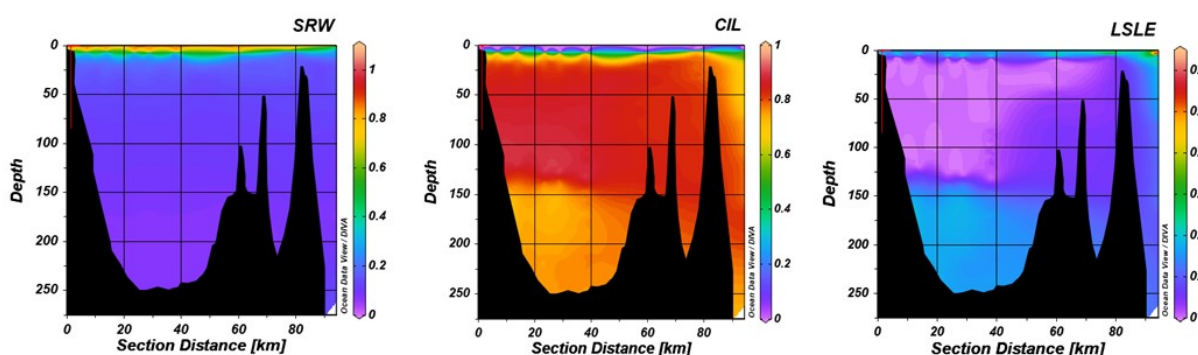


Fig. 3 Vertical sections showing the relative contributions of the Saguenay River (SRW), the St. Lawrence Estuary cold intermediate waters (CIL) and Lower St. Lawrence Estuary bottom waters (LSLE) to the water column structure of the Saguenay Fjord (June 2017). Fractions were estimated using an Optimum Multi-Parameter (OMP) algorithm (Tomczak and Large, 1989; Tomczak, 1981; Mackas and Harrison, 1997). A Variational Analysis (DIVA) interpolation was applied between field data points in Ocean Data View.

3.2 Aqueous pCO_2 and CO_2 flux

The organic alkalinity (acidity) accounted, on average, for 3.5% to 9.5% of the total alkalinity of the Saguenay River and varied annually and seasonally ($-28 \mu\text{mol.kg}^{-1}$ in September 2014, $-38 \mu\text{mol.kg}^{-1}$ in May 2016, $-52 \mu\text{mol.kg}^{-1}$ in June 2017 and $-21 \mu\text{mol.kg}^{-1}$ for November 2017). It was inversely proportional to the salinity of the surface waters of the fjord and became positive but a negligible fraction of $\text{TA}_{(\text{corr})}$ at $S_p > 25$, like in the St. Lawrence Estuary.

Variations of the inorganic carbon chemistry in the Saguenay Fjord water column are described using field data acquired in September 2014, May 2016, June 2017 and November 2017. $p\text{CO}_{2(\text{SW})}$ values were higher at the head of the fjord (i.e. near the Saguenay River mouth) and lower at the mouth of the fjord, although large variations ($236 \mu\text{atm}$ to $769 \mu\text{atm}$ – average $475 \pm 32 \mu\text{atm}$) were observed on a seasonal and yearly basis (Table 2). Computed $p\text{CO}_{2(\text{SW})}$ values were higher in June 2017 ($589 \pm 58 \mu\text{atm}$) and May 2016 ($563 \pm 48 \mu\text{atm}$) than in November 2017 ($420 \pm 28 \mu\text{atm}$) and September 2014 ($362 \pm 31 \mu\text{atm}$). This can be explained by the larger freshwater discharge from the Saguenay River in the spring (i.e. spring freshet, $1400 \text{ m}^3 \text{ s}^{-1}$), compared to the fall/winter ($1100 \text{ m}^3 \text{ s}^{-1}$) (Bourgault et al., 2012). The river drains the Canadian Shield and boreal forest soils, and carries organic acidity released from soil porewaters. As atmospheric $p\text{CO}_{2(\text{air})}$ varied marginally between September 2014 ($395 \mu\text{atm}$) and November 2017 ($407 \mu\text{atm}$), the fjord was generally a source of CO_2 to the atmosphere near its head (i.e. surface $p\text{CO}_2$ values above atmospheric level), while the zone near its mouth was most often a sink (i.e. surface $p\text{CO}_2$ values below atmospheric level) (Fig. 4). An anomaly was observed in November 2017, with a high $p\text{CO}_{2(\text{SW})}$ value ($> 550 \mu\text{atm}$) near the mouth of the fjord. Given the statistics of the box plot presented in Fig. 6, this value appears to be an outlier.

Estimated, area-averaged air-sea CO_2 fluxes within the fjord ranged from $-2.4 \text{ mmol}\cdot\text{m}^{-2}\cdot\text{d}^{-1}$ to $6.6 \text{ mmol}\cdot\text{m}^{-2}\cdot\text{d}^{-1}$ (Fig. 5, Table 3). Near the head of the fjord, fluxes were mostly positive, while values decreased when approaching its mouth. Accordingly, the fjord was divided into two segments to further emphasize this trend. Segment 1 includes the inner basin (30 to 100 km from the mouth of the fjord), while the second segment encompasses the two outer basins (0-30 km from the mouth). Results for $F_{\text{area-avg}}$ can be found in Table 3. Overall, the total area-averaged degassing flux of the fjord adds up to $24 \text{ mmol}\cdot\text{m}^{-2}\cdot\text{d}^{-1}$ (i.e. $9 \text{ mol}\cdot\text{m}^{-2}\cdot\text{yr}^{-1}$). This value compares favorably to other bodies of water around the same latitude such as the Gironde Estuary ($11 \text{ mol}\cdot\text{m}^{-2}\cdot\text{yr}^{-1}$) and the Rhine Estuary ($7 \text{ mol}\cdot\text{m}^{-2}\cdot\text{yr}^{-1}$); Frankignoulle, 1998). In contrast, the degassing flux in the adjacent St. Lawrence Estuary was estimated at between 0.36 and $0.74 \text{ mol}\cdot\text{m}^{-2}\cdot\text{yr}^{-1}$ during the late spring and early summer (Dinauer and Mucci, 2017). This discrepancy can be explained by the low carbonate alkalinity (and buffering capacity) of the Saguenay River waters that flow through the Grenvillian metamorphic and igneous rocks of the Canadian Shield

(Piper et al., 1990), as with most rivers on the north shore of the St. Lawrence Estuary (e.g., Betsiamites, Manicouagan, Romaine; Paul del Giorgio, pers. comm.), and the low productivity of the fjord surface waters because of the very limited light penetration, due to the high chromotropic dissolved organic carbon content of the surface waters (Tremblay and Gagné, 2009; Xie et al., 2012). In contrast, waters of the St. Lawrence River have an elevated carbonate alkalinity ($\sim 1200 \mu\text{mol.kg}^{-1}$), inherited from the Ottawa River that drains through limestone deposits (Telmer and Veizer, 1999). Furthermore, the Estuary is host to multiple seasonal phytoplankton blooms (Levasseur and Therriault, 1987; Zakardjian et al., 2000; Annane et al., 2015) that strongly modulate its trophic status (Dinauer and Mucci, 2018).

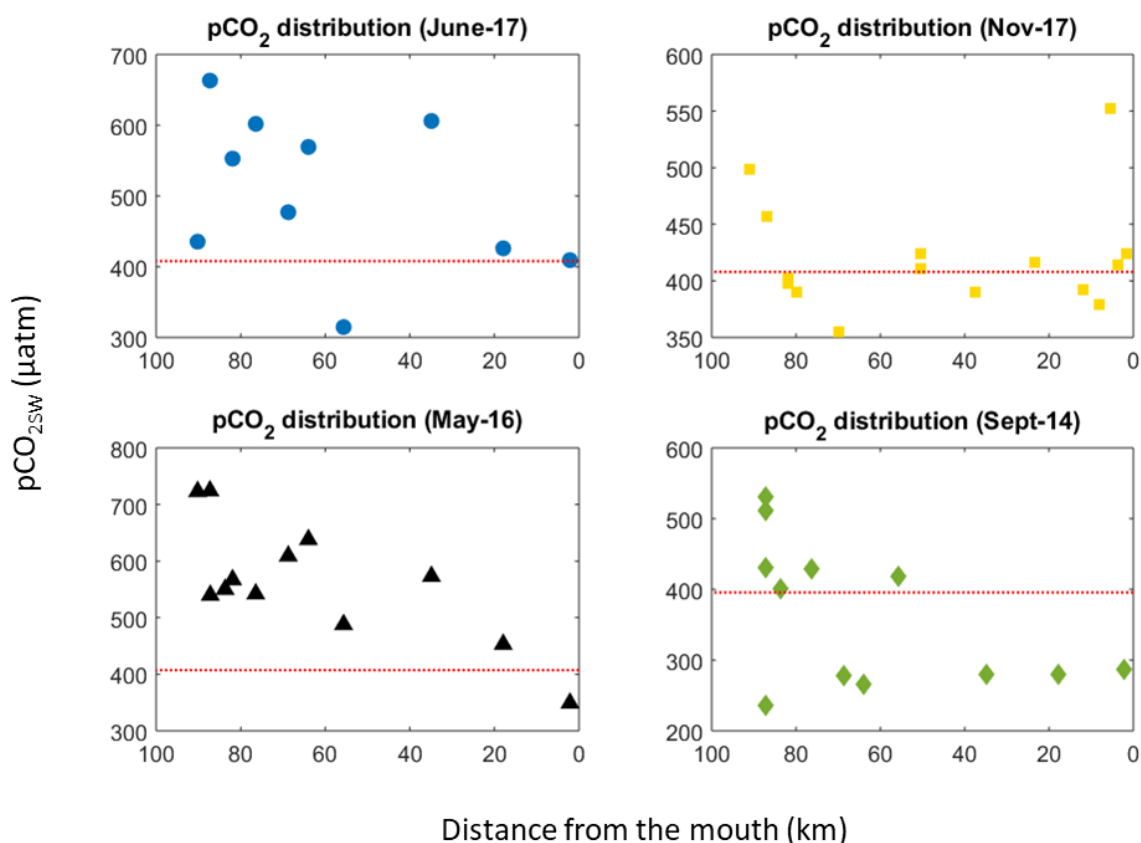


Fig. 4 Spatial distribution of surface-water $p\text{CO}_{2\text{sw}}$ in June 2017, November 2017, May 2016 and September 2014. The red line represents the $p\text{CO}_{2(\text{air})}$ for each year. Data points above the red line indicate that waters are sources of CO_2 to the atmosphere, whereas those below the red line identify waters that are sinks of atmospheric CO_2 .

Sampling Month	pCO ₂ (µatm)	k (cm h ⁻¹)	u (m s ⁻¹)	F (mmol·m ⁻² ·d ⁻¹)
November 2017	420 ± 8.8 (354/552)	3.2 ± 0.01 (2.81/3.37)	4.2	0.49 ± 0.14 (-2.3/5.7)
June 2017	589 ± 16 (346/769)	0.35 ± 0.37 (0.36/0.41)	1.89	0.77 ± 0.06 (-0.2/1.5)
May 2016	563 ± 8.9 (349/724)	1.28 ± 0.005 (1.15/1.40)	3.17	3.08 ± 0.18 (-1.1/6.6)
September 2014	362 ± 8.6 (236/531)	1.48 ± 0.01 (1.34/1.81)	3.71	-0.39 ± 0.16 (-2.4/3.4)

Table 2. Mean, standard error and range of pCO₂, K, u and F in the Saguenay Fjord surface waters. Numbers in parentheses indicate the observed or calculated ranges.

Subsection	November 2017 (N = 15)	June 2017 (N = 10)	May 2016 (N = 12)	September 2014 (N = 12)	Whole fjord
Inner basin	1.4	4.1	21.4	-0.9	23.9
Outer basins	1.7	0.9	1.6	-3.3	

Table 3. Area-averaged, air-sea CO₂ flux (mmol·m⁻²·d⁻¹) estimates for each subsection of the Saguenay Fjord, for N data points, per sampling month. The fjord was divided into two subsections. The 'Inner basin' segment encompasses the 30-100 km section from the mouth of the fjord (Fig. 1b), whereas the 'Outer basins' segment includes the 0-30 km section. The whole fjord CO₂ flux was computed by combining all available flux data over the four sampling months.

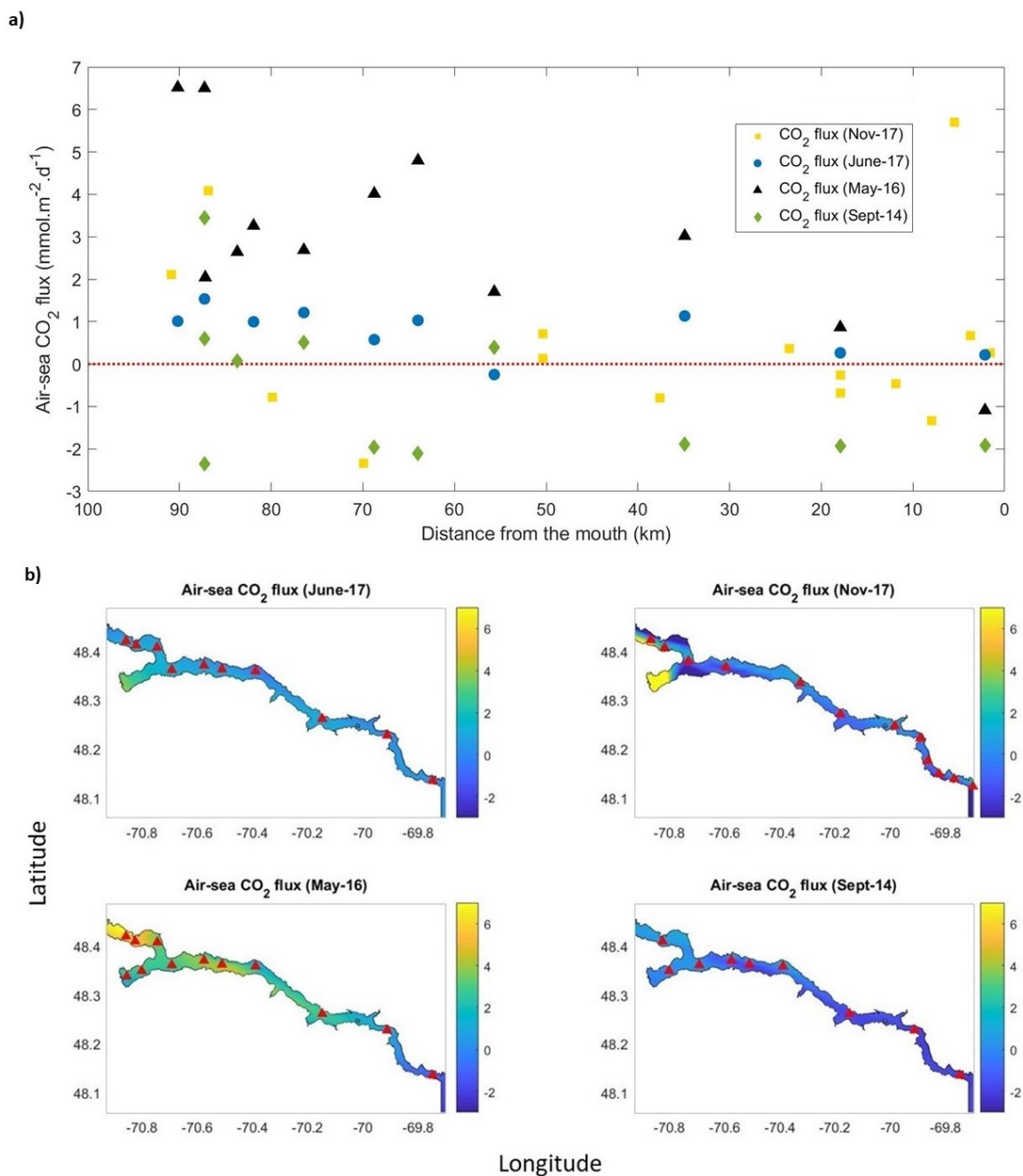


Fig. 5 a) Spatial distribution of air-sea CO₂ flux (mmol·m⁻²·d⁻¹) in the Saguenay Fjord surface waters for all cruises. Data points above the red line indicate sources of CO₂ to the atmosphere, whereas those below the red line are sinks of atmospheric CO₂. **b)** Spatial interpolation of air-sea CO₂ fluxes (mmol·m⁻²·d⁻¹) in the Saguenay Fjord surface waters for all cruises. Red triangles indicate sampling locations.

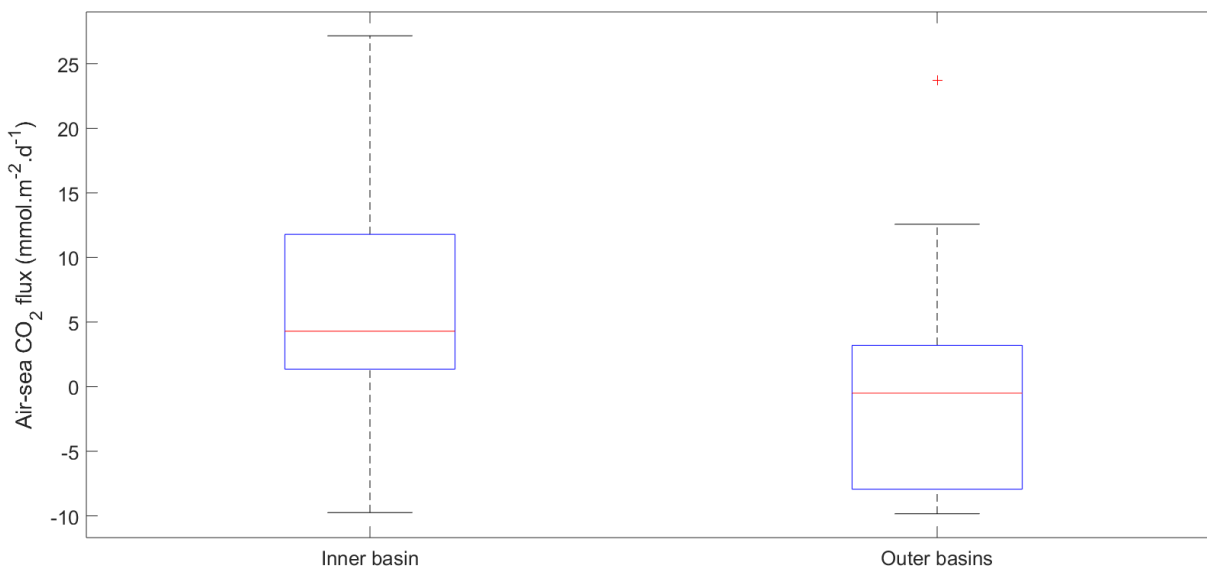


Fig. 6 Box-plot for the air-sea CO₂ fluxes from all data in the two subdivisions of the study area (Inner basin and Outer basins). The red line is the median, the box spans the interquartile range (25-75 percentiles) and the whiskers show the extreme data points not considered outliers. One outlier is identified by the + symbol.

3.3 Water Mixing Model approach

As results of the OMP analysis reveal, LSLE and SLRW have a negligible influence on the water properties in the fjord, except for the latter near the mouth. Additionally, given the relatively small contribution of the LSLE and the similarity of its carbonate chemistry to the CIL, its influence is considered inconsequential on the properties of the mixture. Hence, for most of the fjord, a two-end member model is adequate. A conservative mixing model was constructed based on the chemical properties of the two main source water masses in the fjord (i.e. SRW and the CIL mixture for bottom waters), and the relationship between salinity and $TA_{(corr)}/DIC$, respectively (Fig. 7). The data from the various cruises were superimposed on the model, after correction for the organic alkalinity and normalization to the average water temperature of the sampling period.

Field measurements follow the trend displayed by the mixing model. The fjord appears to be a net source of CO₂ to the atmosphere during periods of high freshwater discharge (i.e. spring freshet) and a net sink at intermediate surface salinities ($5 < S_p < 15$). This is consistent with the

lack of buffering capacity of the freshwater. Furthermore, $p\text{CO}_{2(\text{SW})}$ were normalized to the average surface temperature for each sampling month. Given the short residence time of surface waters in the Saguenay Fjord (~ 1.5 days), the influence of gas exchange across the air-sea interface is negligible on the DIC pool. Likewise, Dinauer and Mucci (2017) reported that the surface waters in the Estuary near Tadoussac are highly supersaturated in CO_2 with respect to the atmosphere and only the highly productive waters of the Lower Estuary manage to draw down the surface $p\text{CO}_2$ to near atmospheric values. In other words, degassing of the metabolic CO_2 accumulated in the river and upper estuary is slow.

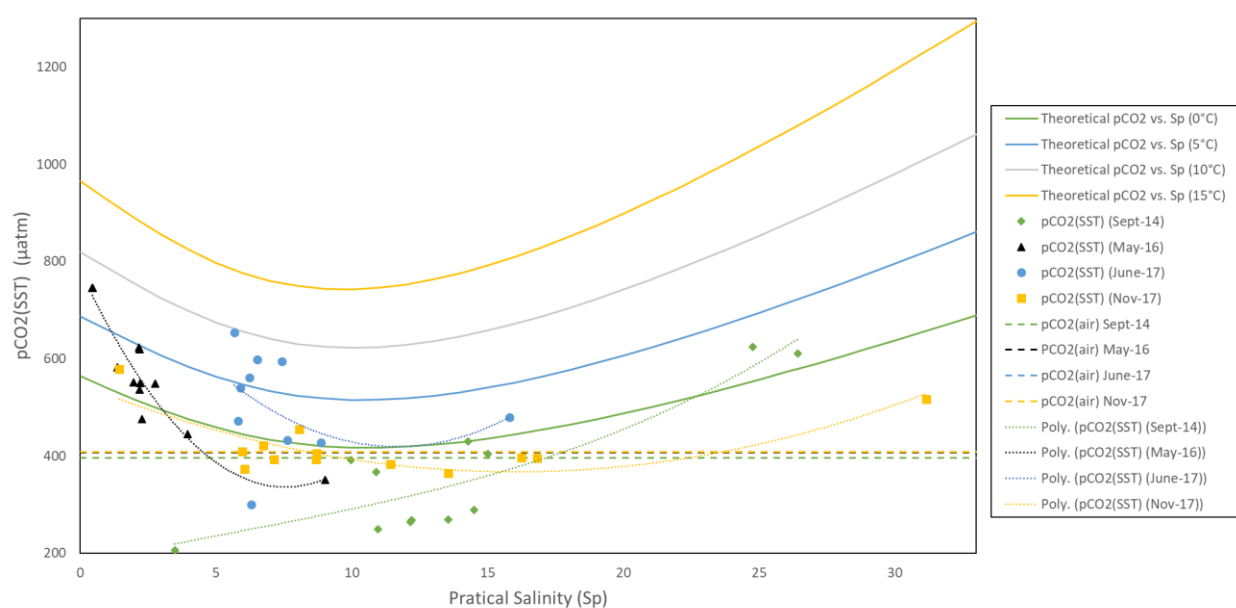


Fig. 7 Results of the conservative, two end-member mixing model for $p\text{CO}_{2(\text{SST})}$ in the Saguenay Fjord surface waters. Dashed lines represent the $p\text{CO}_{2(\text{air})}$ on the sampling months (respectively 396 ppm in September 2014, 407 ppm in May 2016, 408 ppm in June and November 2017).

Hence, changes in $p\text{CO}_2$ at a common temperature primarily reflect changes in DIC. Differences between the model and field measurements can be explained by biological activity (such as microbial respiration and photosynthesis).

In May 2016, the surface waters of the fjord were clearly supersaturated in oxygen (Fig. 8), implying that photosynthesis dominated over respiration, and hence explains the rapid seaward (increasing S_p) decrease in $p\text{CO}_2$ observed in Fig. 7 and the strong negative ΔNDIC (i.e. change in NDIC relative to the saline waters at the head of the fjord) reported in Fig. 9. These results explain

why the $p\text{CO}_{2(\text{SST})}$ decreases faster than the mixing model predicts (Fig. 7), as CO_2 (i.e. DIC) is taken up by photosynthesizing organisms - most likely diatoms (Chassé and Côté, 1991). In June 2017, surface-water oxygen concentrations were close to saturation over a significant portion of the fjord, with a ΔNDIC close to zero except about 40 km from the mouth, where it was strongly negative. This again reflects the $p\text{CO}_2$ trend observed in Fig.7, as the June data follow the mixing model closely.

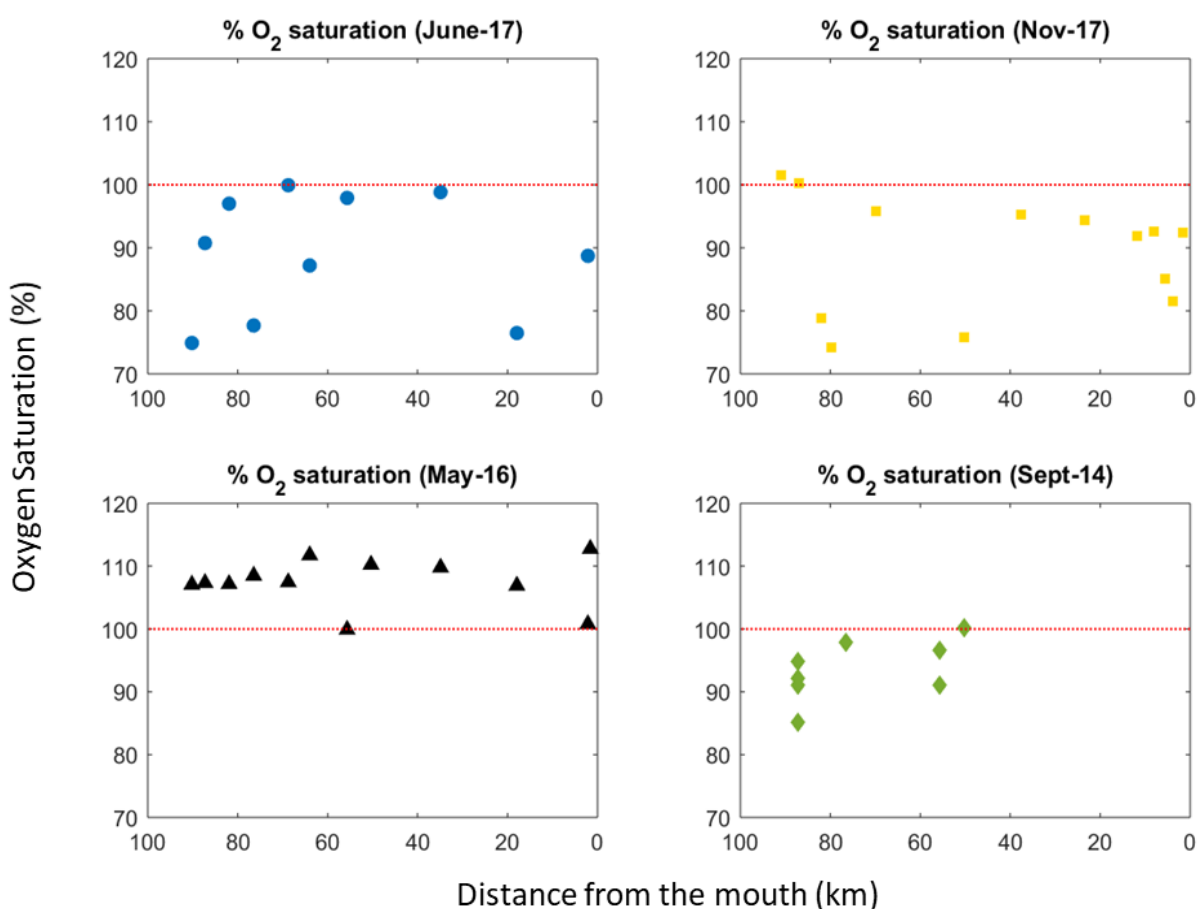


Fig. 8 Spatial distribution of surface-water dissolved O₂ saturation (%) in June 2017, November 2017, May 2016 and September 2014. The red line represents equilibrium with the atmosphere (i.e. 100% saturation). Data points above the red line indicate that waters are supersaturated in O₂, whereas those below the red line identify O₂-undersaturated waters with respect to the atmosphere.

On the other hand, there does not appear to be a clear biological signal in the November 2017 data, as little variation is observed between the measured and modeled $p\text{CO}_2$. Accordingly, Fig. 9 indicates that neither respiration nor photosynthesis dominate during this period as the ΔNDIC varies between weakly positive and negative values, although there seems to be a peak in photosynthetic activity near the mouth with a negative peak in ΔNDIC . Likewise, the $\%O_2$ saturation does not vary significantly, supporting the hypothesis that biological activity has little influence on the surface-water $p\text{CO}_2$ observed during that month (Fig. 8). In contrast to November 2017, the September 2014 data show a slight dominance of respiration (i.e. positive ΔNDIC , especially near the mouth of the fjord), corresponding to the increase in $p\text{CO}_2$ observed in Fig. 7, and hence explaining the slight deviation from the mixing model.

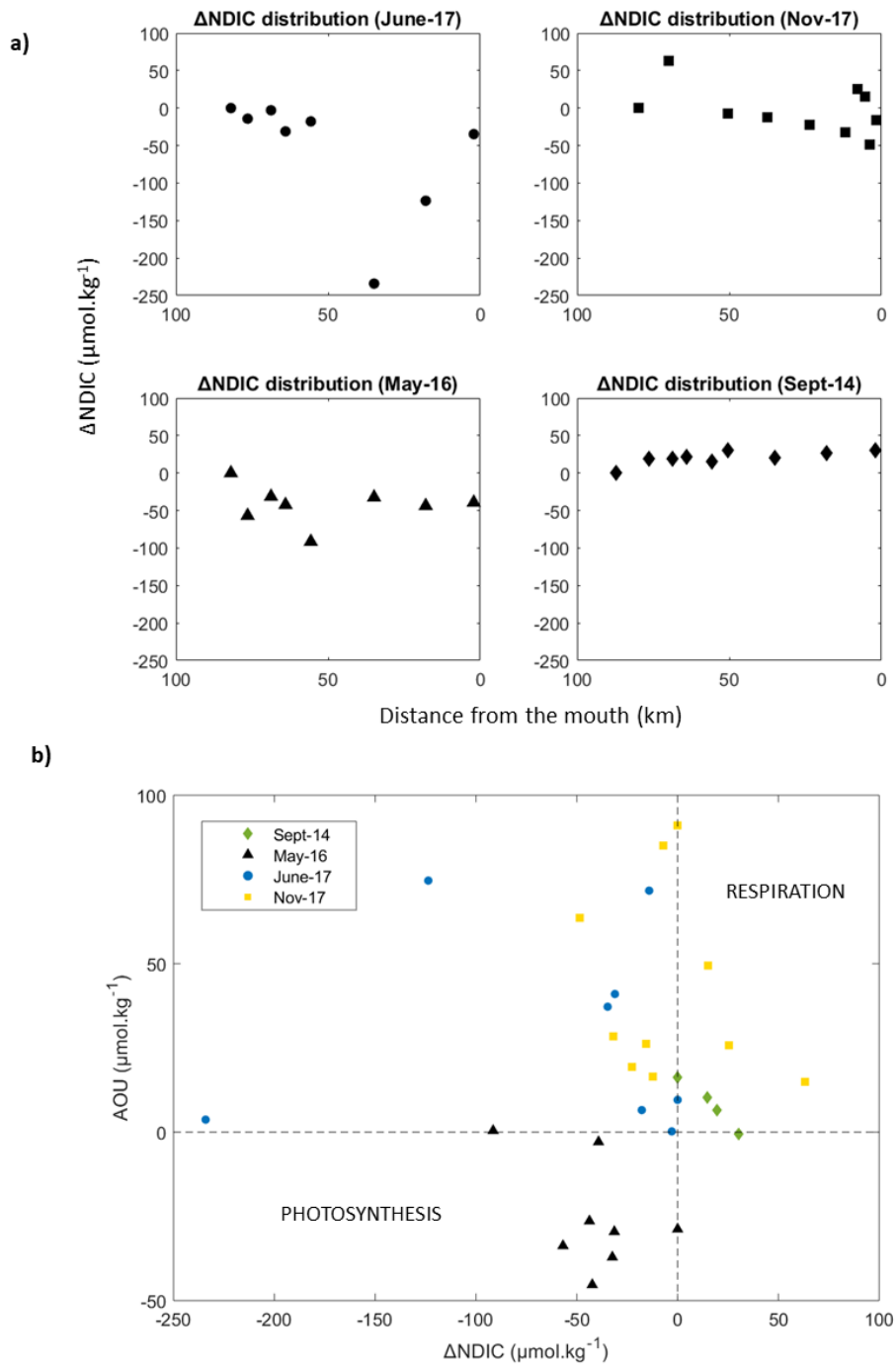


Fig. 9 a) ΔNDIC (i.e. change in NDIC relative to the saline waters at the head of the fjord) distribution in the Saguenay Fjord surface waters. Data were normalized to a common salinity (average for each sampling period) according to Friis *et al.* (2003); **b)** Apparent oxygen utilization (AOU) against ΔNDIC .

4 Summary and conclusions

Results of the OMP analysis reveal that SRW and CIL are the dominant source-water types to the fjord and the structure of its water column. Mixing of marine waters with SRW at the head of the fjord leads to the formation of a brackish surface layer while the CIL replenishes the bottom waters of the fjord. The analysis further unveiled a small contribution to the bottom waters from the LSLE, adding to the complexity of the water structure. The SLRW has a negligible influence on the water properties in the fjord, except near the mouth - sampling of the very turbulent waters directly over the fjord's sill could shed some light on the contribution of the SLRW to the fjord's surface waters.

The fjord serves as a strong source of CO₂ to the atmosphere, with an average yearly outgassing flux of 9 mol·m⁻²·yr⁻¹. There is no plan to manage anthropogenic CO₂ in the fjord or its tributaries, but the intensity of CO₂ degassing is mitigated by the intrusion of brackish water from the Upper St. Lawrence Estuary and spillover as well as mixing with seawater from the Lower Estuary (i.e. Cold Intermediate Layer).

The magnitude and sign of the $\Delta p\text{CO}_2$ across the air-water interface in the Saguenay Fjord, mostly determined by the $p\text{CO}_{2(\text{SW})}$ as $p\text{CO}_{2(\text{air})}$ varies only slightly over the sampling period, are modulated by the freshwater discharge and the salinity of the surface waters. The surface waters of the fjord are a source of CO₂ to the atmosphere at high freshwater discharge, and a sink of CO₂ at intermediate surface salinities ($5 < S_p < 15$), especially at near-freezing temperatures. Biological activity (photosynthesis and respiration) further alters the surface-water $p\text{CO}_2$, with photosynthesis impacting the waters mostly in the spring, and respiration dominating in the fall. This conclusion is further supported by the oxygen saturations observed in the surface waters of the fjord, as well as the ΔNDIC trend. Given the short residence time of surface waters in the Saguenay Fjord (~ 1.5 days), the influence of gas exchange on spatial variations of the $\Delta p\text{CO}_2$ across the air-sea interface is negligible on the DIC pool.

Acknowledgements

We would like to give special thanks to Gilles Desmeules as well as the Captains and crew of the R/V Coriolis II without whom, over the years, this project would not have been possible. Most of the data presented in this study were acquired opportunistically on research cruises funded by grants to A.M. or Canadian colleagues by the Natural Sciences and Engineering Research Council of Canada (NSERC). The work was funded by a Regroupement Stratégique grant from the Fonds Québécois de Recherche Nature et Technologies (FQRNT) to GEOTOP as well as NSERC Discovery and MEOPAR (Canadian Ocean Acidification Research partnership) grants to A.M and H.T. We would like to thank Dr. Jean-Francois Hélie at GEOTOP-UQAM for carrying out the $\delta^{18}\text{O}_{(\text{H}_2\text{O})}$ analyses. We also wish to acknowledge Constance Guignard for cruise preparation and support in the laboratory. Finally, L.D. wishes to thank MEOPAR and the Department of Earth and Planetary Sciences at McGill for financial support in the form of stipends, scholarships and assistantships. Bathymetric data of the fjord was graciously provided by Mélanie Belzile. Figure 3 in this study was created with the ODV Software (Schlitzer, 2015).

ANNEX: Additional information

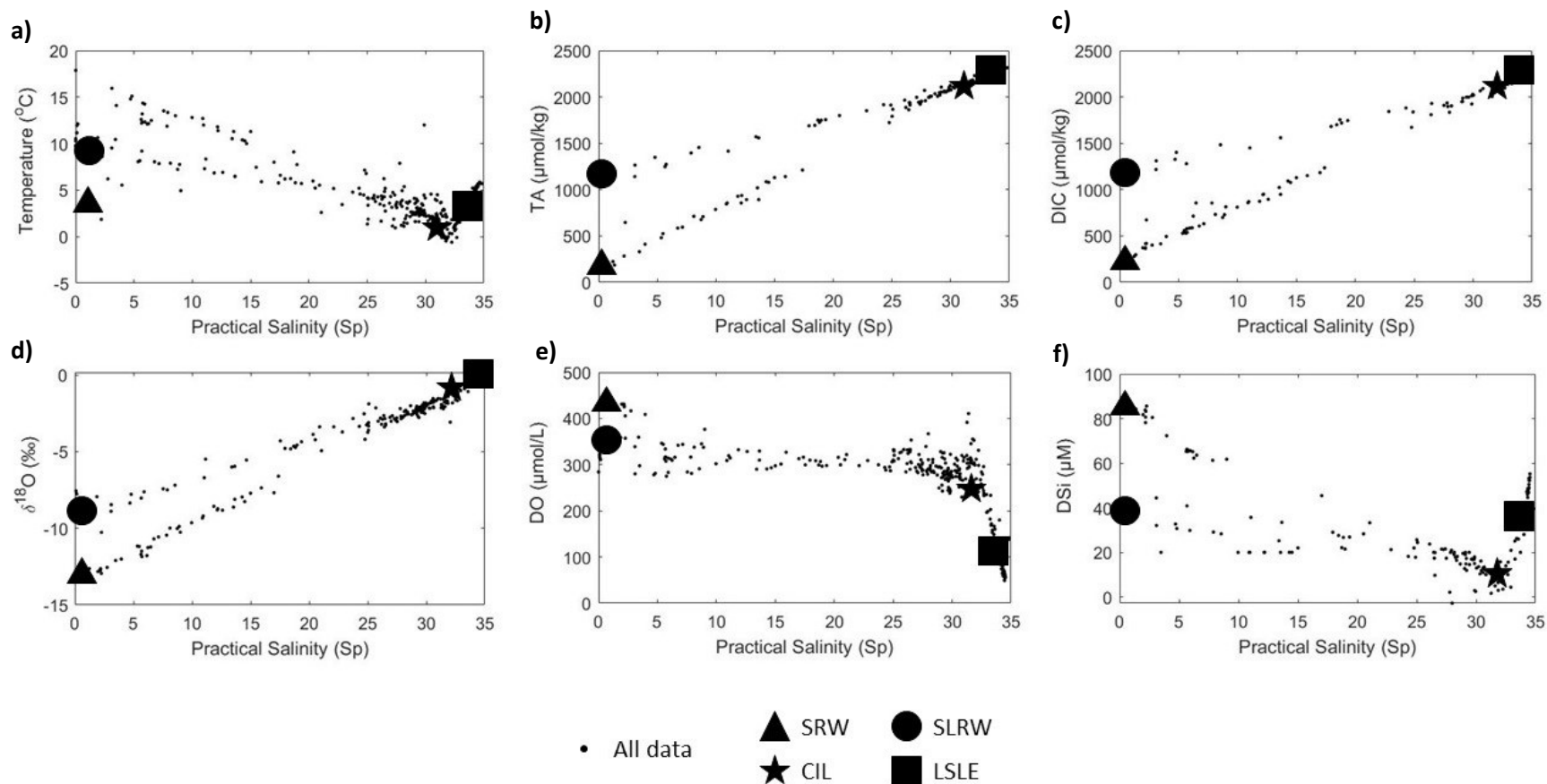


Fig. A Salinity versus a) Temperature, b) Total Alkalinity (TA), c) Dissolved Inorganic Carbon (DIC), d) $\delta^{18}\text{O}_{\text{water}}$, e) Dissolved Oxygen (DO), and f) DSI for data from September 2014, May 2016, June 2017 and November 2017 from R/V Coriolis II cruises. Each large symbol (square, circle, triangle and star) represents distinct source-water masses.

Chapter 3: General summary and conclusions

As the southernmost subarctic fjord in the world, the Saguenay Fjord is an important ecosystem for the study of carbon sources and sinks. Fjords, often considered as miniature oceans, are ideal sites to study terrestrial carbon sequestration and its variation in response to climate change as carbon inputs and outputs are easily quantified in these quasi-closed marine systems. Fjords also serve as natural laboratories to study the migration of the redox gradients, the solubilization and precipitation of major and minor seawater constituents, as well as the cycling of carbon, nitrogen and trace metals. Fjords are therefore unique oceanographic environments and valuable assets of estuarine research.

The objectives of this thesis were to 1) determine the relative contribution of the source-type water masses (i.e., CIL, Saguenay River and other freshwater/marine tributaries) to the water column structure in the fjord using geochemical and isotopic tracers; 2) reconstruct the properties of the water column (temperature, salinity, pH, pCO₂, alkalinity, nutrient concentrations), particularly the surface waters using a conservative mixing model, and to further develop our understanding of bottom-water renewal and circulation in the Saguenay Fjord; and 3) to compare results of a mixing model to field measurements in order to identify factors, other than conservative mixing (i.e. biological activity, gas exchange), that impact the CO₂ fluxes at the air-sea interface throughout the fjord and document the trophic status of the fjord (i.e. whether it is a source of a sink of CO₂ to the atmosphere).

This thesis characterized, for the first time, the spatial distribution of surface-water CO₂ partial pressures (pCO₂) in the fjord, based on a multi-year sampling of carbonate system parameters (salinity, temperature, pH, alkalinity and dissolved inorganic carbon) along the main axis of the fjord in September 2014, May 2016, and June and November 2017. Average air-sea CO₂ fluxes were determined at each sampling station from the difference in the pCO₂ across the air-water interface ($\Delta pCO_2 = pCO_{2(SW)} - pCO_{2(air)}$) and the gas exchange coefficient estimated from the average wind stress for each sampling month over the whole fjord. In addition, area-averaged fluxes for two distinct segments of the fjord (i.e. one encompassing the inner basin, another including the two outer basins) were estimated. The key processes that control spatial variations

of surface-water $p\text{CO}_2$ in the Saguenay Fjord were investigated by examining discrepancies between measured, temperature-normalized $p\text{CO}_{2(\text{SW})}$ values with those obtained using a two end-member conservative mixing model.

Several conclusions emerge from our analysis. Results of the OMP analysis reveal that SRW and CIL are the dominant source waters to the fjord and the structure of its water column. Mixing of marine waters with SRW at the head of the fjord lead to the formation of a brackish surface layer while the CIL replenishes the bottom waters of the fjord. The analysis further unveiled a small contribution to the bottom waters from the LSLE, adding to the complexity of the water structure. The SLRW has a negligible influence on the water properties in the fjord, except near the mouth - sampling of the very turbulent waters directly over the fjord's sill could shed some light on the contribution of the SLRW to the fjord's surface waters.

Biogeochemical processes in the surface waters of the Saguenay Fjord are reflected by the spatial distribution of $p\text{CO}_2$ in these waters (236 μatm to 769 μatm – average $475 \pm 32 \mu\text{atm}$). The Saguenay River, the main tributary to the fjord, is a strong source of CO_2 to the atmosphere, but surface-water values typically decrease seaward as their salinity increases by turbulent mixing with the marine waters below. Nevertheless, overall, the fjord serves as a strong source of CO_2 to the atmosphere, with an average yearly outgassing flux of $9 \text{ mol}\cdot\text{m}^{-2}\cdot\text{yr}^{-1}$. There is no plan to manage anthropogenic CO_2 in the fjord or its tributaries, but the intensity of CO_2 degassing is mitigated by the intrusion of brackish water from the Upper St. Lawrence Estuary and spillover and mixing with seawater from the Lower Estuary (i.e. Cold Intermediate Layer). Hence, the magnitude and sign of the $\Delta p\text{CO}_2$ across the air-water interface in the Saguenay Fjord are modulated by the freshwater discharge and the salinity of the surface waters. The surface waters of the fjord are a source of CO_2 to the atmosphere at high freshwater discharge, and a sink of CO_2 at intermediate surface salinities ($5 < S_p < 15$), especially at near-freezing temperatures. Gas exchange is not expected to play a significant role in modulating surface-water $p\text{CO}_2$ values during the short residence time of the surface waters in the fjord (~ 1.5 day). In contrast, biological activity (photosynthesis and respiration) exert a strong influence on the surface-water $p\text{CO}_2$, with photosynthesis (biological CO_2 uptake) driving down the $p\text{CO}_{2(\text{SW})}$

mostly in the spring, and respiration (metabolic CO₂ production) maintaining or increasing pCO_{2(SW)} in the fall. These observations are supported by the observed oxygen saturations as well as estimated changes in the DIC content of the surface waters (Δ NDIC) along the seaward transect through the fjord.

In addition to outlining the general stratification of the Saguenay Fjord, these results have characterized the surface mixed layer pCO₂ and CO₂ fluxes at the air-sea interface on a temporal and spatial scale and provided a framework for the future study of carbon cycling in fjord waters. More extensive temporal coverage of the fjord is required. Sampling of carbonate system parameters during the fall and winter would greatly improve our understanding of the frequency and mode of deep-water renewals in the water column. Long-term observations and field studies could also provide a more accurate estimate of the temporal evolution of carbon fluxes in the fjord, including the annual average air-sea CO₂ flux, as little to no data are available outside the ice-free season (i.e., winter). In addition to traditional sampling, direct measurements of the pCO_{2(SW)} would be desirable to validate the values we have estimated from other measurable carbonate parameters, especially in view of the strong negative alkalinity (acidity) of the surface waters in the fjord and the uncertainty associated with carbonic acid dissociation constant at low salinities (see Abril et al., 2015; Dinauer and Mucci, 2017; Hunt et al., 2011). Atmospheric sensors combined with eddy correlation measurements should be used to acquire direct measurements of gas exchange at the air-sea interface (see Berg and Pace, 2017; Edson et al., 2011; Else et al., 2011; Marandino et al., 2007; Miller et al., 2010). Finally, a study of biological activity in surface waters should also shed some light on the rates of photosynthesis and microbial respiration that influence the carbon fluxes (organic carbon settling rates and CO₂ fluxes at the air-sea interface) in surface waters.

References

- Aarseth, I., Bjerkli, K., Björklund, K. R., Böe, D., Holm, J. P., Lorentzen-Styr, T. J., ... Thiede, J. (1975). Late Quaternary sediments from Korsfjorden, western Norway. *Sarsia*, 58(1), 43–66. <https://doi.org/10.1080/00364827.1975.10411278>
- Abril, G., Bouillon, S., Darchambeau, F., Teodoru, C. R., Marwick, T. R., Tamooch, F., ... Borges, A. V. (2015). Technical Note: Large overestimation of pCO₂ calculated from pH and alkalinity in acidic, organic-rich freshwater. *Biogeosciences*, 12(1), 67–78. <https://doi.org/10.5194/bg-12-67-2015>
- Annane, S., St-Amand, L., Starr, M., Pelletier, E., and Ferreyra, G. A. (2015). Contribution of transparent exopolymeric particles (TEP) to estuarine particulate organic carbon pool. *Marine Ecology Progress Series*, 529, 17–34. <https://doi.org/10.3354/meps11294>
- Bélangier, C. (2003). Observation and modelling of a renewal event in the Saguenay Fjord, PhD thesis. Univ. du Qué. a Rimouski.
- Bellis, A. (2002). Spectrophotometric determination of pH in estuarine waters using Phenol Red (B.Sc). McGill University, Montreal, Que., Canada.
- Belzile, M., Galbraith, P. S., and Bourgault, D. (2016). Water renewals in the Saguenay Fjord. *Journal of Geophysical Research: Oceans*, 121(1), 638–657. <https://doi.org/10.1002/2015JC011085>
- Berg, P., and Pace, M. L. (2017). Continuous measurement of air–water gas exchange by underwater eddy covariance. *Biogeosciences*, 14(23), 5595–5606. <https://doi.org/10.5194/bg-14-5595-2017>
- Borges, A. V. (2005). Do we have enough pieces of the jigsaw to integrate CO₂ fluxes in the coastal ocean? *Estuaries; Stony Brook*, 28(1), 3–27. <http://dx.doi.org/10.1007/BF02732750>
- Boulton, G. S. (1982). Processes and patterns of glacial erosion. In *Glacial Geomorphology* (pp. 41–87). Springer, Dordrecht. https://doi.org/10.1007/978-94-011-6491-7_2
- Bourgault, D., Galbraith, P. S., and Chavanne, C. (2016). Generation of internal solitary waves by frontally forced intrusions in geophysical flows. *Nature Communications*, 7, 13606. <https://doi.org/10.1038/ncomms13606>
- Bourgault, D., Galbraith, P. S., and Winkler, G. (2012). Exploratory observations of winter oceanographic conditions in the Saguenay Fjord. *Atmosphere-Ocean*, 50(1), 17–30. <https://doi.org/10.1080/07055900.2012.659844>
- Bourgault, D., Janes, D. C., and Galbraith, P. S. (2011). Observations of a large-amplitude internal wave train and its reflection off a steep slope. *Journal of Physical Oceanography*, 41(3), 586–600. <https://doi.org/10.1175/2010JPO4464.1>
- Brewer, P. G., and Peltzer, E. T. (2009). Limits to Marine Life. *Science*, 324(5925), 347–348. <https://doi.org/10.1126/science.1170756>
- Brodie, J. W. (1964). The Fiordland Shelf and Milford Sound. In: *Studies of a southern fiord* (Vol. 17, pp. 15–23). New Zealand Oceanographic Inst. Mem.
- Butman, D., and Raymond, P. A. (2011). Significant efflux of carbon dioxide from streams and rivers in the United States. *Nature Geoscience*, 4(12), 839–842. <https://doi.org/10.1038/ngeo1294>

- Cai, W.-J. (2011). Estuarine and coastal ocean carbon paradox: CO₂ sinks or sites of terrestrial carbon incineration? *Annual Review of Marine Science*, 3(1), 123–145. <https://doi.org/10.1146/annurev-marine-120709-142723>
- Cai, W.-J., and Wang, Y. (1998). The chemistry, fluxes, and sources of carbon dioxide in the estuarine waters of the Satilla and Altamaha Rivers, Georgia. *Limnology and Oceanography*, 43(4), 657–668. <https://doi.org/10.4319/lo.1998.43.4.0657>
- Caldeira, K. (2005). Ocean model predictions of chemistry changes from carbon dioxide emissions to the atmosphere and ocean. *Journal of Geophysical Research*, 110(C9). <https://doi.org/10.1029/2004JC002671>
- Chassé, R., and Côté, R. (1991). Aspects of winter primary production in the upstream section of Saguenay Fjord. *Hydrobiologia*, 215(3), 251–260. <https://doi.org/10.1007/BF00764860>
- Chester, R. (1990). *Marine geochemistry*. Allen and Unwin, Australia.
- Clayton, T. D., and Byrne, R. H. (1993). Spectrophotometric seawater pH measurements: total hydrogen ion concentration scale calibration of m-cresol purple and at-sea results. *Deep Sea Research Part I: Oceanographic Research Papers*, 40(10), 2115–2129. [https://doi.org/10.1016/0967-0637\(93\)90048-8](https://doi.org/10.1016/0967-0637(93)90048-8)
- Côté, R., and Lacroix, G. (1978). Tidal variability of physical, chemical and biological characteristics in the Saguenay Fjord, *J. Fish. Res. Bd. Can.* (35), 338–345.
- Côté, R., and Lacroix, G. (1978). Capacité photosynthétique du phytoplancton de la couche aphotique dans le fjord du Saguenay. Photosynthetic capacity of deep phytoplankton in the Saguenay Fjord. *Internationale Revue Der Gesamten Hydrobiologie Und Hydrographie*, 63(2), 233–246. <https://doi.org/10.1002/iroh.19780630209>
- d'Anglejan, B. F., and Smith, E. C. (1973). Distribution, transport, and composition of suspended matter in the St. Lawrence Estuary. *Canadian Journal of Earth Sciences*, 10(9), 1380–1396. <https://doi.org/10.1139/e73-128>
- Deflandre, B., Mucci, A., Gagné, J.-P., Guignard, C., and Sundby, B. (2002). Early diagenetic processes in coastal marine sediments disturbed by a catastrophic sedimentation event. *Geochimica et Cosmochimica Acta*, 66(14), 2547–2558. [https://doi.org/10.1016/S0016-7037\(02\)00861-X](https://doi.org/10.1016/S0016-7037(02)00861-X)
- Deflandre, B., Sundby, B., Gremare, A., Lefrancois, L., and Gagné, J.-P. (2000). Effects of sedimentary microenvironments on the vertical distributions of O₂ and DOC in coastal marine sediments: Scales of variability. *EOS: Trans. Am. Geophys. Union* 80(49), 115.
- Dickie, L. M., and Trites, R. W. (1983). The Gulf of St. Lawrence.
- Dickson, A. G., Sabine, C. L., Christian, J. R., Barger, C. P., and North Pacific Marine Science Organization (Eds.). (2007). *Guide to best practices for ocean CO₂ measurements*. Sidney, BC: North Pacific Marine Science Organization.
- Dinauer, A., and Mucci, A. (2017). Spatial variability in surface-water pCO₂ and gas exchange in the world's largest semi-enclosed estuarine system: St. Lawrence Estuary (Canada). *Biogeosciences; Katlenburg-Lindau*, 14(13), 3221–3237. <http://dx.doi.org/10.5194/bg-14-3221-2017>
- Dinauer, A., and Mucci, A. (2018). Distinguishing between physical and biological controls on the spatial variability of pCO₂: A novel approach using OMP water mass analysis (St. Lawrence, Canada). *Marine Chemistry*. <https://doi.org/10.1016/j.marchem.2018.03.007>

- Dionne, J.-C., and Occhietti, S. (1996). Aperçu du Quaternaire à l'embouchure du Saguenay, Québec. *Géographie physique et Quaternaire*, 50(1), 5–34. <https://doi.org/10.7202/033072ar>
- Doney, S. C., Fabry, V. J., Feely, R. A., and Kleypas, J. A. (2009). Ocean acidification: the other CO₂ problem. *Annual Review of Marine Science*, 1(1), 169–192. <https://doi.org/10.1146/annurev.marine.010908.163834>
- Douglas, N. K., and Byrne, R. H. (2017). Achieving accurate spectrophotometric pH measurements using unpurified meta-cresol purple. *Marine Chemistry*, 190, 66–72. <https://doi.org/10.1016/j.marchem.2017.02.004>
- Drainville, G., and Québec (Province). Ministère de l'industrie et du commerce. (1968). Le fjord du Saguenay: contribution à l'océanographie. Ministère de l'industrie et du commerce.
- Edson, J. B., Fairall, C. W., Bariteau, L., Zappa, C. J., Cifuentes-Lorenzen, A., McGillis, W. R., ... Helmig, D. (2011). Direct covariance measurement of CO₂ gas transfer velocity during the 2008 Southern Ocean Gas Exchange Experiment: Wind speed dependency. *Journal of Geophysical Research: Oceans*, 116(C4). <https://doi.org/10.1029/2011JC007022>
- El-Sabh, M. I., and Silverberg, N. (1990). The St. Lawrence Estuary: Introduction. In *Oceanography of a Large-Scale Estuarine System* (pp. 1–9). Springer, New York, NY. https://doi.org/10.1007/978-1-4615-7534-4_1
- Else, B. G. T., Papakyriakou, T. N., Galley, R. J., Drennan, W. M., Miller, L. A., and Thomas, H. (2011). Wintertime CO₂ fluxes in an Arctic polynya using eddy covariance: Evidence for enhanced air-sea gas transfer during ice formation. *Journal of Geophysical Research: Oceans*, 116(C9). <https://doi.org/10.1029/2010JC006760>
- Epstein, S., and Mayeda, T. (1953). Variation of O₁₈ content of waters from natural sources. *Geochimica et cosmochimica acta*, 4(5), 213–224.
- Frankignoulle, M. (1998). Carbon dioxide emission from European Estuaries. *Science*, 282(5388), 434–436. <https://doi.org/10.1126/science.282.5388.434>
- Friis, K., Körtzinger, A., and Wallace, D. W. R. (2003). The salinity normalization of marine inorganic carbon chemistry data. *GRL Geophysical Research Letters*, 30(2).
- Gade, H. G., and Edwards, A. (1980). Deep water renewal in fjords. In H. J. Freeland, D. M. Farmer, and C. D. Levings (Eds.), *Fjord Oceanography* (pp. 453–489). Boston, MA: Springer US. https://doi.org/10.1007/978-1-4613-3105-6_43
- Gade, H. G. (1968). Horizontal and vertical exchanges and diffusion in the water masses of the Oslo fjord. *Helgoländer Wissenschaftliche Meeresuntersuchungen*, 17(1–4), 462–475. <https://doi.org/10.1007/BF01611247>
- Galbraith, P. S. (2006). Winter water masses in the Gulf of St. Lawrence. *Journal of Geophysical Research: Oceans*, 111(C6). <https://doi.org/10.1029/2005JC003159>
- Galbraith, P. S., Bourgault, D., and Belzile, M. (2018). Circulation et renouvellement des masses d'eau du fjord du Saguenay. *Le Naturaliste canadien*, 142(2), 36. <https://doi.org/10.7202/1047147ar>
- Gattuso, J.-P., Frankignoulle, M., and Wollast, R. (1998). Carbon and carbonate metabolism in coastal aquatic ecosystems. *Annual Review of Ecology and Systematics*, 29, 405–434.

- Gilbert, D., and Pettigrew, B. (1997). Interannual variability (1948-1994) of the CIL core temperature in the Gulf of St. Lawrence. *Canadian Journal of Fisheries and Aquatic Sciences*, 54(S1), 57-67.
- Gilbert, R. (1985). Quaternary glaciomarine sedimentation interpreted from seismic surveys of fjords on Baffin Island, N.W.T. *ARCTIC*, 38(4), 271–280. <https://doi.org/10.14430/arctic2146>
- Glasby, G. P. (1978). Sedimentation and sediment geochemistry of Caswell, Nancy and Milford Sounds. In *Fiord Studies: Caswell and Nancy Sounds, New Zealand*. (Vol. 79). N.Z. Ocean. Inst. Mem.
- Grasshoff, K., Kremling, K., and Ehrhardt, M. (1999) Methods of seawater Analysis – Third Edition, completely revised and extended version, Seawater Analysis Wiley-VCH, 600pp., doi:10.1002/9783527613984, 1999.
- Gratton, Y., Mertz, G., and Gagné, J. A. (1988). Satellite observations of tidal upwelling and mixing in the St. Lawrence estuary. *Journal of Geophysical Research: Oceans*, 93(C6), 6947–6954. <https://doi.org/10.1029/JC093iC06p06947>
- Guérin, F., Abril, G., Serça, D., Delon, C., Richard, S., Delmas, R., ... Varfalvy, L. (2007). Gas transfer velocities of CO₂ and CH₄ in a tropical reservoir and its river downstream. *Journal of Marine Systems*, 66(1), 161–172. <https://doi.org/10.1016/j.jmarsys.2006.03.019>
- Holtedahl, H. (1967). Notes on the formation of fjords and fjord-valleys. *Geografiska Annaler. Series A, Physical Geography*, 49, 188. <https://doi.org/10.2307/520887>
- Hönisch, B., Ridgwell, A., Schmidt, D. N., Thomas, E., Gibbs, S. J., Sluijs, A., ... Williams, B. (2012). The Geological Record of Ocean Acidification. *Science*, 335(6072), 1058–1063.
- Hunt, C. W., Salisbury, J. E., and Vandemark, D. (2011). Contribution of non-carbonate anions to total alkalinity and overestimation of pCO₂ in New England and New Brunswick rivers. *Biogeosciences*, 8(10), 3069–3076. <https://doi.org/10.5194/bg-8-3069-2011>
- Jiang, L.-Q., Cai, W.-J., and Wang, Y. (2008). A comparative study of carbon dioxide degassing in river- and marine-dominated estuaries. *Limnology and Oceanography*, 53(6), 2603–2615. <https://doi.org/10.4319/lo.2008.53.6.2603>
- Juul-Pedersen, T., Arendt, K., Mortensen, J., Blicher, M., Søgaard, D., and Rysgaard, S. (2015). Seasonal and interannual phytoplankton production in a sub-Arctic tidewater outlet glacier fjord, SW Greenland. *Marine Ecology Progress Series*, 524, 27–38. <https://doi.org/10.3354/meps11174>
- Karstensen, J. (2013). OMP (Optimum Multiparameter) analysis - USER GROUP. Retrieved from <http://omp.geomar.de/>
- Karstensen, J., and Tomczak, M. (1998). Age determination of mixed water masses using CFC and oxygen data. *Journal of Geophysical Research: Oceans*, 103(C9), 18599–18609. <https://doi.org/10.1029/98JC00889>
- Lansard, B., Mucci, A., Miller, L. A., Macdonald, R. W., and Gratton, Y. (2012). Seasonal variability of water mass distribution in the southeastern Beaufort Sea determined by total alkalinity and $\delta^{18}\text{O}$: water masses in the Beaufort Sea. *Journal of Geophysical Research: Oceans*, 117(C3), n/a-n/a. <https://doi.org/10.1029/2011JC007299>

- Lavoie, D., Simard, Y., and Saucier, F. J. (2000). Aggregation and dispersion of krill at channel heads and shelf edges: the dynamics in the Saguenay - St. Lawrence Marine Park. *Canadian Journal of Fisheries and Aquatic Sciences*, 57(9), 1853–1869. <https://doi.org/10.1139/f00-138>
- Levasseur, M. E., and Therriault, J.-C. (1987). Phytoplankton biomass and nutrient dynamics in a tidally induced upwelling: the role of the $\text{NO}_3:\text{SiO}_4$ ratio. *Mar. Ecol. Prog. Ser.*, 11.
- Locat, J., and Levesque, C. (2009). Le fjord du Saguenay : une physiographie et un registre exceptionnels. *Revue des sciences de l'eau*, 22(2), 135. <https://doi.org/10.7202/037479ar>
- Louchouart, P., Lucotte, M., Canuel, R., Gagné, J.-P., and Richard, L.-F. (1997). Sources and early diagenesis of lignin and bulk organic matter in the sediments of the Lower St. Lawrence Estuary and the Saguenay Fjord. *Marine Chemistry*, 58(1), 3–26. [https://doi.org/10.1016/S0304-4203\(97\)00022-4](https://doi.org/10.1016/S0304-4203(97)00022-4)
- Louchouart, P., Lucotte, M., and Farella, N. (1999). Historical and geographical variations of sources and transport of terrigenous organic matter within a large-scale coastal environment. *Organic Geochemistry*, 30(7), 675–699. [https://doi.org/10.1016/S0146-6380\(99\)00019-4](https://doi.org/10.1016/S0146-6380(99)00019-4)
- Lüthi, D., Le Floch, M., Bereiter, B., Blunier, T., Barnola, J.-M., Siegenthaler, U., ... Stocker, T. F. (2008). High-resolution carbon dioxide concentration record 650,000–800,000 years before present. *Nature*, 453(7193), 379–382. <https://doi.org/10.1038/nature06949>
- Mackas, D. L., Denman, K. L., and Bennett, A. F. (1987). Least squares multiple tracer analysis of water mass composition. *Journal of Geophysical Research: Oceans*, 92(C3), 2907–2918. <https://doi.org/10.1029/JC092iC03p02907>
- Mackas, D. L., and Harrison, P. J. (1997). Nitrogenous nutrient sources and sinks in the Juan de Fuca Strait/Strait of Georgia/Puget Sound Estuarine System: Assessing the potential for eutrophication. *Estuarine, Coastal and Shelf Science*, 44(1), 1–21. <https://doi.org/10.1006/ecss.1996.0110>
- Marandino, C. A., Bruyn, W. J. D., Miller, S. D., and Saltzman, E. S. (2007). Eddy correlation measurements of the air/sea flux of dimethylsulfide over the North Pacific Ocean. *Journal of Geophysical Research: Atmospheres*, 112(D3). <https://doi.org/10.1029/2006JD007293>
- Miller, S. D., Marandino, C., and Saltzman, E. S. (2010). Ship-based measurement of air-sea CO_2 exchange by eddy covariance. *Journal of Geophysical Research: Atmospheres*, 115(D2).
- Millero, F. J. (1986). The pH of estuarine waters. *Limnology and Oceanography*, 31(4), 839–847. <https://doi.org/10.4319/lo.1986.31.4.0839>
- Molvær, J. (1980). Deep Water renewals in the Frierfjord - An intermittently anoxic basin. In *Fjord Oceanography* (pp. 531–537). Springer, Boston, MA. https://doi.org/10.1007/978-1-4613-3105-6_48
- Mucci, A., Bernier, G., and Guignard, C. (2015). Mercury remobilization in Saguenay Fjord (Quebec, Canada) sediments: Insights following a mass-flow event and its capping efficiency. *Applied Geochemistry*, 54, 13–26. <https://doi.org/10.1016/j.apgeochem.2014.12.008>
- Mucci, A., Boudreau, B., and Guignard, C. (2003). Diagenetic mobility of trace elements in sediments covered by a flash flood deposit: Mn, Fe and As. *Applied Geochemistry*, 18(7), 1011–1026. [https://doi.org/10.1016/S0883-2927\(02\)00207-X](https://doi.org/10.1016/S0883-2927(02)00207-X)

- Mucci, A., Richard, L.-F., Lucotte, M., and Guignard, C. (2000). The differential geochemical behavior of arsenic and phosphorus in the water column and sediments of the Saguenay Fjord Estuary, Canada. *Aquatic Geochemistry*, 6(3), 293–324. <https://doi.org/10.1023/A:1009632127607>
- Musée du Fjord. (2002). Saguenay River water circulation. Retrieved from http://www.virtualmuseum.ca/sgc-cms/expositions-exhibitions/fjord/english/f_intro_e.html
- Orr, J.C. (2011) Recent and future changes in ocean carbonate chemistry. In: Gattuso J-P, Hansson L (eds) Ocean acidification. Oxford University Press, Oxford, pp 41–66
- Orr, J. C., Epitalon, J.-M., Dickson, A. G., and Gattuso, J.-P. (2018). Routine uncertainty propagation for the marine carbon dioxide system. *Marine Chemistry*, 207, 84–107. <https://doi.org/10.1016/j.marchem.2018.10.006>
- Park, P. K. (1969). Oceanic CO₂ System: an evaluation of ten methods of investigation. *Limnology and Oceanography*, 14(2), 179–186. <https://doi.org/10.4319/lo.1969.14.2.0179>
- Pelletier, E., and Lebel, J. (1979). Hydrochemistry of dissolved inorganic carbon in the St. Lawrence Estuary (Canada). *Estuarine and Coastal Marine Science*, 9(6), 785–795. [https://doi.org/10.1016/S0302-3524\(79\)80011-0](https://doi.org/10.1016/S0302-3524(79)80011-0)
- Perret, D., Locat, J., and Leroueil, S. (1995). Strength development with burial in fine-grained sediments from the Saguenay Fjord, Quebec. *Canadian Geotechnical Journal*, 32(2), 247–262.
- Pierrot, D. E. Lewis, and D. W. R. Wallace. (2006). MS Excel Program Developed for CO₂ System Calculations. ORNL/CDIAC-105a. Carbon Dioxide Information Analysis Center, Oak Ridge National Laboratory, U.S. Department of Energy, Oak Ridge, Tennessee. doi: 10.3334/CDIAC/otg.CO2SYS_XLS_CDIAC105a
- Pinet, N., Brake, V., Campbell, C., and Duchesne, M. (2011). Seafloor and shallow subsurface of the St. Lawrence River Estuary. *Geoscience Canada*, 38(1). Retrieved from <https://journals.lib.unb.ca/index.php/GC/article/view/18589>
- Piper, D. J. W., Mudie, P. J., Fader, G. B., Josenhans, H. W., MacLean, B., and Vilks, G. (1990). Quaternary Geology, Chapter 10. In *Geology of the Continental Margin of Eastern Canada*. (Vol. 2, pp. 475–607). Geological Survey of Canada, Geology of Canada.
- Pocklington, R., and Leonard, J. D. (1979). Terrigenous Organic Matter in Sediments of the St. Lawrence Estuary and the Saguenay Fjord. *Journal of the Fisheries Research Board of Canada*, 36(10), 1250–1255. <https://doi.org/10.1139/f79-179>
- Pocklington, R. (1976). Terrigenous organic matter in surface sediments from the Gulf of St. Lawrence. *Journal of the Fisheries Research Board of Canada*, 33(1), 93–97. <https://doi.org/10.1139/f76-011>
- Pritchard, D. W. (1967). *Observations of Circulation in Coastal Plain Estuaries*. In: *Estuaries*. G.H. Lauff, ed. Washington: A.A.A.S. Publication 83, pp. 37-44.
- Rhein, M., Rintoul, R. S., Aoki, S., Campos, E., Chambers, D., Feely, R., and Gulev, S. (2013). Observations: ocean. In *Climate Change 2013: The Physical Science Basis. Contribution of Working Group 1 to the Fifth Assessment Report of the Intergovernmental Panel on Climate Change* (pp. 1–62). Cambridge University Press. Retrieved from http://www.ipcc.ch/pdf/assessment-report/ar5/wg1/WG1AR5_Chapter03_FINAL.pdf

- Richards, F. A. (1965) Anoxic basins and fjords. *Chemical oceanography Vol. 1*. Academic Press, New York, USA, pp. 611-645
- Robert-Baldo, G. L., Morris, M. J., and Byrne, R. H. (1985). Spectrophotometric determination of seawater pH using phenol red. *Analytical Chemistry*, 57(13), 2564–2567. <https://doi.org/10.1021/ac00290a030>
- Rysgaard, S., Mortensen, J., Juul-Pedersen, T., Sørensen, L. L., Lennert, K., Søgaard, D. H., ... Bendtsen, J. (2012). High air–sea CO₂ uptake rates in nearshore and shelf areas of Southern Greenland: Temporal and spatial variability. *Marine Chemistry*, 128–129, 26–33. <https://doi.org/10.1016/j.marchem.2011.11.002>
- Saucier, F. J., and Chassé, J. (2000). Tidal circulation and buoyancy effects in the St. Lawrence Estuary. *Atmosphere-Ocean*, 38(4), 505–556. <https://doi.org/10.1080/07055900.2000.9649658>
- Schafer, C. T., Smith, J. N., and Seibert, G. (1983). Significance of natural and anthropogenic sediment inputs to the Saguenay Fjord, Quebec. *Sedimentary Geology*, 36, 177–194. [https://doi.org/10.1016/0037-0738\(83\)90008-8](https://doi.org/10.1016/0037-0738(83)90008-8)
- Schafer, C. T., Smith, J. N., and Loring, D. H. (1980). Recent sedimentation events at the head of Saguenay Fjord, Canada. *Environmental Geology*, 3(3), 139–150. <https://doi.org/10.1007/BF02473489>
- Schlitzer, R. (2015). Ocean Data View, [odv. awi. de](http://odv.awi.de).
- Schubel, J. R., and Hirschberg, D. J. (1978). Estuarine graveyards, climatic change, and the importance of the estuarine environment. In M. L. Wiley (Ed.), *Estuarine Interactions* (pp. 285–303). Academic Press. <https://doi.org/10.1016/B978-0-12-751850-3.50024-8>
- Seibert, G. H., Trites, R. W., and Reid, S. J. (1979). Deepwater exchange processes in the Saguenay Fjord. *Journal of the Fisheries Research Board of Canada*, 36(1), 42–53. <https://doi.org/10.1139/f79-006>
- Skei, J. M. (1983). Geochemical and sedimentological considerations of a permanently anoxic fjord — Framvaren, south Norway. *Sedimentary Geology*, 36(2), 131–145. [https://doi.org/10.1016/0037-0738\(83\)90006-4](https://doi.org/10.1016/0037-0738(83)90006-4)
- Skei, J. M. (1983). Permanently anoxic marine basins: Exchange of substances across boundaries. *Ecological Bulletins*, (35), 419–429.
- Smethier, W. M. (1981). Vertical mixing rates in fjords determined using radon and salinity as tracers. *Estuarine, Coastal and Shelf Science*, 12(2), 131–153. [https://doi.org/10.1016/S0302-3524\(81\)80092-8](https://doi.org/10.1016/S0302-3524(81)80092-8)
- Smith, J. N., and Schafer, C. T. (1985). A 20th century record of seasonally-modulated sediment accumulation rates in a Canadian fjord based on Pb-210 measurements. *J. Quaternary Res.* 27: 232-247.
- Smith, J. N., and Walton, A. (1980). Sediment accumulation rates and geochronologies measured in the Saguenay Fjord using the Pb-210 dating method. *Geochimica et Cosmochimica Acta*, 44(2), 225–240. [https://doi.org/10.1016/0016-7037\(80\)90134-9](https://doi.org/10.1016/0016-7037(80)90134-9)
- Smith, R. W., Bianchi, T. S., Allison, M., Savage, C., and Galy, V. (2015). High rates of organic carbon burial in fjord sediments globally. *Nature Geoscience*, 8(6), 450–453. <https://doi.org/10.1038/ngeo2421>

- Stacey, M. W., and Gratton, Y. (2001). The energetics and tidally induced reverse renewal in a two-silled fjord. *Journal of Physical Oceanography*, 31(6), 1599–1615. [https://doi.org/10.1175/1520-0485\(2001\)031<1599:TEATIR>2.0.CO;2](https://doi.org/10.1175/1520-0485(2001)031<1599:TEATIR>2.0.CO;2)
- St-Onge, G., and Hillaire-Marcel, C. (2001). Isotopic constraints of sedimentary inputs and organic carbon burial rates in the Saguenay Fjord, Quebec. *Marine Geology*, 176(1–4), 1–22. [https://doi.org/10.1016/S0025-3227\(01\)00150-5](https://doi.org/10.1016/S0025-3227(01)00150-5)
- St-Onge, G., Mulder, T., Piper, D. J. W., Hillaire-Marcel, C., and Stoner, J. S. (2004). Earthquake and flood-induced turbidites in the Saguenay Fjord (Québec): a Holocene paleoseismicity record. *Quaternary Science Reviews*, 23(3), 283–294. <https://doi.org/10.1016/j.quascirev.2003.03.001>
- Strain, P. M., and Tan, F. C. (1979). Carbon and oxygen isotope ratios in the Saguenay Fjord and the St Lawrence Estuary and their implications for paleoenvironmental studies. *Estuarine and Coastal Marine Science*, 8(2), 119–126. [https://doi.org/10.1016/0302-3524\(79\)90067-7](https://doi.org/10.1016/0302-3524(79)90067-7)
- Strøm, K. M. (1936). Land-locked Waters. *Nwske Videnak.-Akad., MaandNaturv. Kl. 1958, No. 7, 85 pp.*
- Sundby, B., and Loring, D. H. (1978). Geochemistry of suspended particulate matter in the Saguenay Fjord. *Canadian Journal of Earth Sciences*, 15(6), 1002–1011. <https://doi.org/10.1139/e78-108>
- Syvitski, J. P. M., Burrell, D. C., and Skei, J. M. (1987). *Fjords: Processes and Products*. Springer Science and Business Media.
- Syvitski, J. P. M., and Murray, J. W. (1981). Particle interaction in fjord suspended sediment. *Marine Geology*, 39(3), 215–242. [https://doi.org/10.1016/0025-3227\(81\)90073-6](https://doi.org/10.1016/0025-3227(81)90073-6)
- Syvitski, J. P. M., and Schaefer, C. (1996). Evidence for an earthquake-triggered basin collapse in Saguenay Fjord, Canada. *Sedimentary Geology*, 104(1), 127–153. [https://doi.org/10.1016/0037-0738\(95\)00125-5](https://doi.org/10.1016/0037-0738(95)00125-5)
- Syvitski, J. P. M., and Praeg, D. (1989). Quaternary sedimentation in the St. Lawrence Estuary and adjoining areas, Eastern Canada: An overview based on high-resolution seismic stratigraphy. *Géographie Physique et Quaternaire*, 43(3), 291–310. <https://doi.org/10.7202/032784ar>
- Telmer, K., and Veizer, J. (1999). Carbon fluxes, pCO₂ and substrate weathering in a large northern river basin, Canada: Carbon isotope perspectives. *Chemical Geology*, 159, 61–86. [https://doi.org/10.1016/S0009-2541\(99\)00034-0](https://doi.org/10.1016/S0009-2541(99)00034-0)
- Therriault, J. C., de Ladurantaye, R., and Ingram, R. G. (1984). Particulate matter exchange across a Fjord sill. *Estuarine, Coastal and Shelf Science*, 18(1), 51–64. [https://doi.org/10.1016/0272-7714\(84\)90006-4](https://doi.org/10.1016/0272-7714(84)90006-4)
- Therriault, J.-C., Ladurantaye, R. de, and Ingram, R. G. (1980). Particulate matter exchange processes between the St. Lawrence Estuary and the Saguenay Fjord. In *Fjord Oceanography* (pp. 363–366). Springer, Boston, MA. https://doi.org/10.1007/978-1-4613-3105-6_31
- Therriault, J.-C., and Lacroix, G. (1975). Penetration of the deep layer of the Saguenay Fjord by surface waters of the St. Lawrence Estuary. *Journal of the Fisheries Research Board of Canada*, 32(12), 2373–2377. <https://doi.org/10.1139/f75-273>

- Tollo, R., Corriveau, L., Mclelland, J., and J. Bartholomew, M. (2004). Proterozoic tectonic evolution of the Grenville orogen in North America: An introduction. *Memoir of the Geological Society of America*, 197, 1–18. <https://doi.org/10.1130/0-8137-1197-5.1>
- Tomczak, M. (1981). An analysis of mixing in the frontal zone of South and North Atlantic Central Water off North-West Africa. *Progress in Oceanography*, 10(3), 173–192. [https://doi.org/10.1016/0079-6611\(81\)90011-2](https://doi.org/10.1016/0079-6611(81)90011-2)
- Tomczak, M. (1999). Potential Vorticity as a tracer in quantitative water mass analysis. *International WOCE Newsletter*, (36), 6–10.
- Tomczak, M., and Large, D. G. B. (1989). Optimum multiparameter analysis of mixing in the thermocline of the eastern Indian Ocean. *Journal of Geophysical Research: Oceans*, 94(C11), 16141–16149. <https://doi.org/10.1029/JC094iC11p16141>
- Tremblay, L., and Gagné, J.-P. (2009). Organic matter distribution and reactivity in the waters of a large estuarine system. *Marine Chemistry*, 116(1–4), 1–12. <https://doi.org/10.1016/j.marchem.2009.09.006>
- Wang, Z. A., Bienvenu, D. J., Mann, P. J., Hoering, K. A., Poulsen, J. R., Spencer, R. G. M., and Holmes, R. M. (2013). Inorganic carbon speciation and fluxes in the Congo River. *Geophysical Research Letters*, 40(3), 511–516. <https://doi.org/10.1002/grl.50160>
- Wanninkhof, R. (2014). Relationship between wind speed and gas exchange over the ocean revisited. *Limnology and Oceanography: Methods*, 12(6), 351–362. <https://doi.org/10.4319/lom.2014.12.351>
- Wanninkhof, R. (1992). Relationship between wind speed and gas exchange over the ocean. *Journal of Geophysical Research: Oceans*, 97(C5), 7373–7382. <https://doi.org/10.1029/92JC00188>
- Weiss, R. F. (1974). Carbon dioxide in water and seawater: the solubility of a non-ideal gas. *Marine Chemistry*, 2(3), 203–215. [https://doi.org/10.1016/0304-4203\(74\)90015-2](https://doi.org/10.1016/0304-4203(74)90015-2)
- Weiss, R. F., and Price, B. A. (1980). Nitrous oxide solubility in water and seawater. *Marine Chemistry*, 8(4), 347–359. [https://doi.org/10.1016/0304-4203\(80\)90024-9](https://doi.org/10.1016/0304-4203(80)90024-9)
- Xie, H., Aubry, C., Bélanger, S., and Song, G. (2012). The dynamics of absorption coefficients of CDOM and particles in the St. Lawrence estuarine system: Biogeochemical and physical implications. *Marine Chemistry*, 128–129, 44–56. <https://doi.org/10.1016/j.marchem.2011.10.001>
- Zakardjian, B., Gratton, Y., and Vézina, A. (2000). Late spring phytoplankton bloom in the Lower St. Lawrence Estuary: the flushing hypothesis revisited. *Marine Ecology Progress Series*, 192, 31–48. <https://doi.org/10.3354/meps192031>
- Zeebe RE, Wolf-Gladrow D. 2001. *CO₂ in Seawater: Equilibrium, Kinetics, Isotopes*. Amsterdam: Elsevier Science, B.V. 346 pp.